Technical Report Documentation Page

1. Report No. FHWA/TX-08/0-5506-2	2. Government Accession No.	3. Recipient's Catalog No.
4. Title and Subtitle Numerical Modeling of Narrow MSE Walls with Extensible Reinforcements		5. Report Date February 2008 6. Performing Organization Code
7. Author(s) Kuo-Hsin Yang, Jorge G. Zornberg, and Stephen G. Wright		8. Performing Organization Report No. 0-5506-2
9. Performing Organization Name and Address Center for Transportation Research The University of Texas at Austin 3208 Red River, Suite 200 Austin, TX 78705-2650		10. Work Unit No. (TRAIS) 11. Contract or Grant No. 0-5506
12. Sponsoring Agency Name and Address Texas Department of Transportation Research and Technology Implementation Office P.O. Box 5080 Austin, TX 78763-5080		13. Type of Report and Period Covered Technical Report, Fall 2005 to Fall 2007 14. Sponsoring Agency Code

15. Supplementary Notes
Project performed in cooperation with the Texas Department of Transportation and the Federal Highway Administration.

16. Abstract

The Texas Department of Transportation (TxDOT) is experiencing wider use of Mechanically Stabilized Earth (MSE) Walls placed adjacent to an existing stable wall. In numerous cases, the space (width) available for the new wall is less than the width established in current guidelines for stand-alone MSE walls. This wall system combining an existing stable wall and a new MSE wall with constrained space is referred as a narrow MSE wall system. Although walls have already been designed and constructed for such applications, the actual mechanism of the narrow MSE wall system is still unclear. Accordingly, the current research project was undertaken. A detailed review of relevant literature has been complied and design considerations have been proposed and presented in the companion project report.

This report presents a series of numerical analyses of narrow MSE wall systems. The numerical models were conducted using finite element and limit equilibrium methods. Both models were validated by the results of centrifuge testing. The proposed procedure of numerical modeling narrow MSE wall system serves as a basis of practical applications. Furthermore, a series of parametric studies was performed based on the validity of the calibrated numerical models. The behaviors and mechanics of the narrow MSE wall systems were investigated and studied through the parametric studies. The results of parametric studies allow us to define the actual location of failure surface in a narrow MSE wall and to understand the mechanism causing the external failure when wall aspect ratio below 0.25.

17. Key Words Numerical modeling, Finite element, Limit equilibrium, Centrifuge test, Narrow Mechanically stabilized earth (MSE) walls, Retaining walls, Design, Geotechnical engineering.	18. Distribution Statement No restrictions. This document is available to the public through the National Technical Information Service, Springfield, Virginia 22161; www.ntis.gov.

19. Security Classif. (of report) Unclassified	20. Security Classif. (of this page) Unclassified	21. No. of pages 72	22. Price

Form DOT F 1700.7 (8-72) Reproduction of completed page authorized

Numerical Modeling of Narrow MSE Walls with Extensible Reinforcements

Kuo-Hsin Yang
Jorge G. Zornberg
Stephen G. Wright

CTR Technical Report:	0-5506-2
Report Date:	February 2008
Project:	0-5506
Project Title:	Numerical Modeling of a Narrow MSE Wall with Extensible Reinforcements
Sponsoring Agency:	Texas Department of Transportation
Performing Agency:	Center for Transportation Research at The University of Texas at Austin

Project performed in cooperation with the Texas Department of Transportation and the Federal Highway Administration.

Center for Transportation Research
The University of Texas at Austin
3208 Red River
Austin, TX 78705

www.utexas.edu/research/ctr

Disclaimers

Author's Disclaimer: The contents of this report reflect the views of the authors, who are responsible for the facts and the accuracy of the data presented herein. The contents do not necessarily reflect the official view or policies of the Federal Highway Administration or the Texas Department of Transportation (TxDOT). This report does not constitute a standard, specification, or regulation.

Patent Disclaimer: There was no invention or discovery conceived or first actually reduced to practice in the course of or under this contract, including any art, method, process, machine manufacture, design or composition of matter, or any new useful improvement thereof, or any variety of plant, which is or may be patentable under the patent laws of the United States of America or any foreign country.

Engineering Disclaimer

NOT INTENDED FOR CONSTRUCTION, BIDDING, OR PERMIT PURPOSES.

Project Engineer: Stephen G. Wright
Professional Engineer License State and Number: Texas No. 49007
P. E. Designation: Research Supervisor

Acknowledgments

The authors express appreciation to the TxDOT Project Director and members of the Project Monitoring Committee

Table of Contents

1. Introduction 1
1.1 Background 1
1.2 Objectives 2

2. Review of Centrifuge Test of Narrow MSE Wall 5
2.1 Centrifuge Modeling 5
2.2 Test Equipment 6
2.2.1 Centrifuge 6
2.2.2 Strong Box 6
2.2.3 Video System 7
2.3 Material Characteristics 7
2.3.1 Backfill 7
2.3.2 Reinforcements 9
2.4 Scope of the Testing Program 11
2.5 Results 12
2.6 Conclusions 15

3. Finite Element Analysis 17
3.1 Finite Element Model 17
3.1.1 Initial Geometry and Boundary Condition 17
3.1.2 Backfill Model and Material Properties 18
3.1.3 Reinforcement and Facing Elements and Material Properties 19
3.1.4 Interface Models and Material Properties 20
3.2 Results 20
3.2.1 Working Stress Condition 21
3.2.2 Failure Condition 22
Failure Characteristics 22
Development of Tensile Forces in the Reinforcements 25
3.2.3 Development of a Zero Pressure Zone at the Interface 25
3.3 Lessons Learned from Finite Element Simulations 27
3.4 Conclusions 28

4. Limit Equilibrium Analysis 29
4.1 Limit Equilibrium Approach 29
4.1.1 Modeling of Wall Systems 29
4.1.2 Modeling of Backfill in MSE and Stale Wall 30
4.1.3 Modeling of Reinforcement 31
Tensile Forces 31
Pullout Resistance 31
Overlap Layer of Reinforcement 33
Orientation of Reinforcement Tension 33
4.1.4 Search for Noncircular Failure Surface 33
4.2 Results 34
4.2.1 Factor of Safety versus G-Level 34
4.2.2 Location of the Failure Surface 36

4.2.3 Normal Stress along Failure Surface 39
4.3 Parametric Studies 40
4.3.1 Effect of the Reinforcement Pullout Resistance 41
4.3.2 Effect of Tensile Force Suggested by FHWA Design Guidelines 42
4.4 Effect of Aspect Ratio on the location of the Failure Surface 44
4.5 Conclusions 47

5. Overall Conclusions 49

References 51

Appendix A. Modeling a Flexible Wall Face 53
A.1 Introduction 53
A.2 Possible Methods 53
A.3 Plate Elements 54
A.4 Normalization of EA and EI 54
A.4.1 Normalization of EA 55
A.4.2 Normalization of EI 56
A.5 Parametric Study 57
A.6 Summary 59
A.7 Example of Calculation 60

List of Figures

Figure 1.1: Illustration of proposed narrow MSE wall in front of a stable face 1
Figure 2.1: Centrifuge at the University of Colorado 6
Figure 2.2: A schematic of the testing set up (Woodruff 2003) 7
Figure 2.3: Particle size distribution for Monterey No. 30 sand (Arriaga 2003) 8
Figure 2.4: Stress-strain curve of Monterey No. 30 sand (Woodruff 2003) 9
Figure 2.5: Pellon true-grid retrieved after centrifuge testing (Woodruff 2003) 10
Figure 2.6: Test results from a wide-width tensile test (Woodruff 2003) 11
Figure 2.7: Photographic images from centrifuge: (a) Initial condition (gravity); (b) Working Stresses (10g); (c) Before Failure (41g); (d) Failure condition (41g) (Woodruff, 2003) 13
Figure 2.8: An example of compound failure at Test 2b (Woodruff, 2003) 14
Figure 3.1: Wall geometry of Test 2b: (a) Finite element setup and initial mesh; (b) Picture from centrifuge at initial condition 17
Figure 3.2: Stress-strain curves for drained triaxial tests on Monterey #30 sand 18
Figure 3.3: Comparison of displacement at working stress condition: (a) Location A; (b) Location B 21
Figure 3.4: Comparison of displacement: (a) displacement contour from finite element simulation; (b) Image from centrifuge. 22
Figure 3.5: Development of tensile force along each layer of reinforcements 24
Figure 3.6: Comparison of breakage of reinforcements: (a) Results from finite element simulation; (b) Image of reinforcement. 25
Figure 3.7: Distribution of normal stress along interface face: (a) Test 2b; (b) Test 5c 26
Figure 3.8: Stress points of Test 2b at failure condition 28
Figure 4.1: Wall model of Test 2b 30
Figure 4.2: Schematic of assumed distribution of tensile stresses in the reinforcement 31
Figure 4.3: Values of the vertical stress influence factors at the top and bottom of the wall plotted as a function of the wall aspect ratio (Kniss 2007) 33
Figure 4.4: Factor of safety versus g-level for Test 2b 35
Figure 4.5: Factor of safety versus g-level for Test 2a 35
Figure 4.6: Factor of safety versus g-level for Test 3a 36
Figure 4.7: Location of failure surface for Test 2b 37
Figure 4.8: Location of failure surface for Test 2a 38
Figure 4.9: Location of failure surface for Test 3b 39

Figure 4.10: Normal stress along the failure surface 40
Figure 4.11: The factor of safety and location of failure surface by ignoring the slope part of tensile force in reinforcement 41
Figure 4.12: Variation of stress ratio with depth in a MSE wall (Elias et al, 2001) 43
Figure 4.13: The factor of safety and location of failure surface by using the tensile force suggested by the FHWA Design Guidelines 44
Figure 4.14: Illustration of inclination angle of failure surface 45
Figure 4.15: Inclination angles of failure surfaces versus various aspect ratios 46
Figure 4.16: Normalized inclination angles 47

FigureA.1: Distribution of nodes and stress points in plate elements (a) 5-node (b) 3-node 54
Figure A.2: Axial loading of a beam 55
Figure A.3: Example of simply supported beam with distributed load P 56
Figure A.4: Finite element model for flexible wall face 57
Figure A.5: Graph used to determine the values of N_{EI} for a plate 58
Figure A.6: Graph used to determine the values of NEA for a plate 59

List of Tables

Table 1.1: Summary of wall failure modes and design methods 2
Table 2.1: Centrifuge scaling relations (Ko 1988) 5
Table 2.2: Unconfined tensile strength of reinforcements (Woodruff 2003) 10
Table 2.3: Summary of test scope (Woodruff, 2003) 12
Table 2.4: A summary of the test results (Woodruff, 2003) 15
Table 3.1: Material properties for sand backfill 19
Table 3.2: Material properties for reinforcement and facing elements 20
Table A.1: Summary of values for normalized axial and bending stiffnesses 60

1. Introduction

1.1 Background

As the population increases and development of urban areas is subject to increasing constraints, transportation demand has led to widening of existing highways to improve traffic flow. An increasingly common practice involves building mechanically stabilized earth (MSE) walls in front of previously stabilized walls (or shored walls). However, due to the high cost of additional right-of-way and often limited space available, construction of earth retaining walls is often done under constrained spaces. This leads to retaining walls that are narrower than those recommended in current design guidelines. A narrow wall system, herein, is referred to as a MSE wall with an aspect ratio (L/H) below 0.70 that is placed in front of a stabilized wall. An example of a narrow wall system is illustrated in Figure 1.1

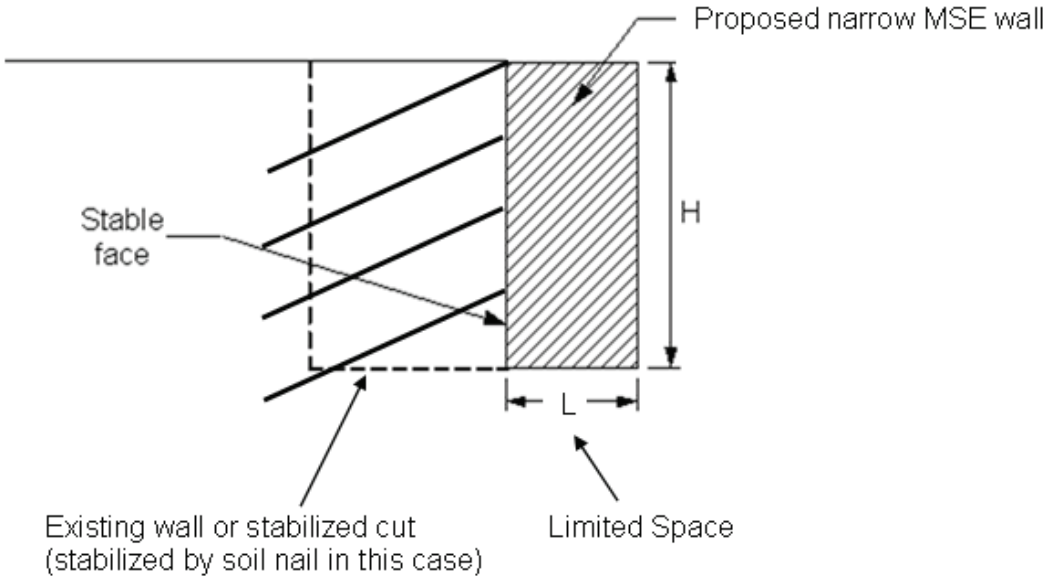

Figure 1.1: Illustration of proposed narrow MSE wall in front of a stable face

Because of space constraints and the interaction with stabilized walls, various studies have suggested that the internal and external behaviors of narrow MSE walls are different from those of traditional walls. Studies on this topic include Frydman and Keissar (1987) and Take and Valsangkar (2001), who performed centrifuge tests, Leshchinsky and Hu (2003) and Lawson and Yee (2005), who conducted limit equilibrium analyses, and the results in the companion report (Kniss et al., 2007), who used finite element analyses to study the earth pressures of narrow walls. They all concluded that, due to arching effect, the earth pressure coefficient decreased as wall aspect ratio, ratio of wall width to wall height (L/H), decreased. This implies that the traditional method using conventional earth pressure equations to calculate the factor of safety against breakage may not be appropriate for narrow walls.

Woodruff (2003) performed a series of centrifuge model tests on reinforced soil walls adjacent to a stable face. Two important observations were drawn from this experimental study:

- The failure planes are bilinear and have an inclination less than the theoretical Rankine linear failure plane. This suggests that traditional methods that assume the Rankine failure plane to evaluate the factor of safety against pullout is not applicable for narrow walls.
- When the wall aspect ratio decreased below 0.3, the failure mode changed from internal failure to external failure. Woodruff (2003) reported that the external failure initiated from a "trench" at the interface between the reinforced backfill and stable wall. This trench had a tendency to pull MSE wall away from the stable wall resulting in external failure. These results imply that, in addition to issues about internal stability, the external stability for narrow walls may require different considerations than those for conventional walls.

A summary, as reported and recommended for various sources, of dominant failure modes and corresponding design methods for various aspect ratios is provided in Table 1.1

Table 1.1: Summary of wall failure modes and design methods

Wall Aspect Ratio	L/H<0.3	0.3<L/H<0.6	0.7>L/H>0.6	L/H>0.7
Failure Mode	External	Compund	Internal	Internal
Design Method	Cement Stabilized Wall (suggested by Reinforced Earth Company)	FHWA SMSE Wall Design Guidelines (Morrison et al. 2006)		FHWA MSE Wall Design Guidelines (Elias et al., 2001)

Although the Federal Highway Administration (FHWA) design guidelines for shored mechanically stabilized earth (SMSE) wall systems is suggested for the design of MSE walls with aspect ratios from 0.3 to 0.7 (Morrison et al. 2006), several important characteristics of narrow MSE walls are not considered in these guidelines. For example, the guidelines make no allowances for a reduction of earth pressure due to arching effect. Also, the design based on these design guidelines appears conservative and uneconomical when applying it to the design of narrow walls. Finally, the SMSE wall guidelines suggest neglecting the calculation of external stability, which contradicts the evidence of failure mode observed in centrifuge tests.

1.2 Objectives

The main purpose of this report is to investigate the characteristics of a narrow wall, which, as known, differs from those of a conventional wall with an aspect ratio larger than 0.7. The experimental bases for this study are on centrifuge test results (Woodruff, 2003) and finite element simulations. Specifically, two questions observed from Woodruff's centrifuge tests are expected to be answered:

- Define the location of failure surface in narrow walls. Based on this knowledge, designers will be able to evaluate the factor of safety against pullout for narrow walls.

- Understand the mechanics and development of trench that initiates the external failure of narrow walls. Based on this information, design can be improved to prevent external failures.

This report presents the numerical simulations of centrifuge tests for narrow MSE walls. Specifically, the finite element and limit equilibrium methods are used in the analyses. The results of numerical simulations are compared to the results from centrifuge tests. The goals of numerical studies are:

- Validate finite element and limit equilibrium models for simulating a narrow MSE wall. These established models can serve as an example for future design of a narrow wall by using the tool of finite element or limit equilibrium methods.
- Understand the sensitivity of parameters in a narrow wall by the numerical simulations. Some valuable information, like mobilization of stress in backfill and in reinforcements that can not be obtain directly from centrifuge test, can be obtained from numerical simulations. This information helps in understanding the mechanics and characteristics of a narrow wall. The finite element simulation is used to identify the mechanics of the "trench" that appears to trigger failure of narrow walls. The limit equilibrium simulation is performed to understand the location of failure surface and the global stability of narrow walls.

The organization of this report includes a description of the centrifuge tests (Chapter 2) and finite element simulations (Chapter 3), and limit equilibrium analyses (Chapter 4) of centrifuge tests. The results of numerical simulations are compared to centrifuge tests. Observations and conclusions are presented in the last section of each chapter. Overall summary and conclusions are listed in Chapter 5. Note that all the centrifuge tests and numerical simulations presented in this report are for a deformable/ flexible narrow MSE wall or a narrow MSE wall reinforced with extensible reinforcements. The applications made by this report can only be extended to flexible walls or walls reinforced with extensible reinforcements with careful considerations.

2. Review of Centrifuge Test of Narrow MSE Wall

2.1 Centrifuge Modeling

In this chapter, review is presented of a series of centrifuge model tests on reinforced soil walls adjacent to a stable face. The tests were performed by Woodruff (2003) under the supervision of Dr. Zornberg at the University of Colorado at Boulder. Centrifuge modeling is useful to gain understanding of soil structures over the last 20 years. The reason for choosing the centrifuge model is because of its advantage over small- and full-scale models. Small-scale models do not replicate the prototype stress conditions, while full-scale models require time, labor and cost for construction and are not suitable for evaluation of repeatability.

When conducting centrifuge modeling, it is important to know the uses, the scaling laws, and the limitations to centrifuge testing. Centrifuge model tests are conducted at an increased acceleration level (g-level) to simulate the actual field conditions. In order to use centrifuge modeling for the prediction of prototype behavior, knowledge of the scaling laws is essential. Increasing the acceleration level during centrifuge modeling, N times that of natural gravity leads to relations summarized in Table 2.1 (Ko, 1988), assuming that the backfill material in the model is the same as that in the prototype. Based on the relation in Table 2.1, it is worth mentioning that the ultimate tensile strength and stiffness of the planar reinforcements for centrifuge models should be reduced N times in relation to the ultimate tensile strength and stiffness of the reinforcements in prototype. In addition to the scaling laws, centrifuge modeling is subjected to sources of error. Some sources of error include the varying acceleration field with the centrifuge model, the stress paths in the model, boundary effects and scale effects (Zornberg 1997).

Table 2.1: Centrifuge scaling relations (Ko 1988)

Quantity	Prototype	Model
Length	N	1
Area	N^2	1
Volume	N^3	1
Velocity	1	1
Acceleration	1	N
Mass	N^3	1
Force	N^2	1
Energy	N^3	1
Stress	1	1
Strain	1	1
Mass Density	1	1
Energy Density	1	1
Time (Dynamic)	N	1
Time (Diffusion)	N^2	1
Time (Creep)	1	1
Frequency	1	N

2.2 Test Equipment

2.2.1 Centrifuge

The centrifuge models presented by Woodruff were tested in the 400g-ton centrifuge at the University of Colorado at Boulder. The centrifuge has a 5.5m radius and is able to carry a 1.22m square package with a height of 0.91 m weighing up to 2 tons. The maximum centrifugal force centrifuge is around 200 times the acceleration of gravity. Figure 2.1 shows a picture of the centrifuge at the University of Colorado.

2.2.2 Strong Box

The aluminum strong box used to contain the models has the dimension of 1.1 m wide by 1.2 m long and 0.4 m deep. Two sides of the box were made of aluminum and another two sides were made of Plexi-glass. The Plexi-glass allowed viewing the profile of the walls during testing. Mylar sheets were attached to the walls to minimize the boundary effect or the friction along the walls. Rigid aluminum dividers were added to the strong box to represent the existing stable wall (shoring system) behind the MSE walls. The divider created four subdivisions and allowed up to four different walls to be tested at the same time. The strong box schematic can be seen in Figure 2.2.

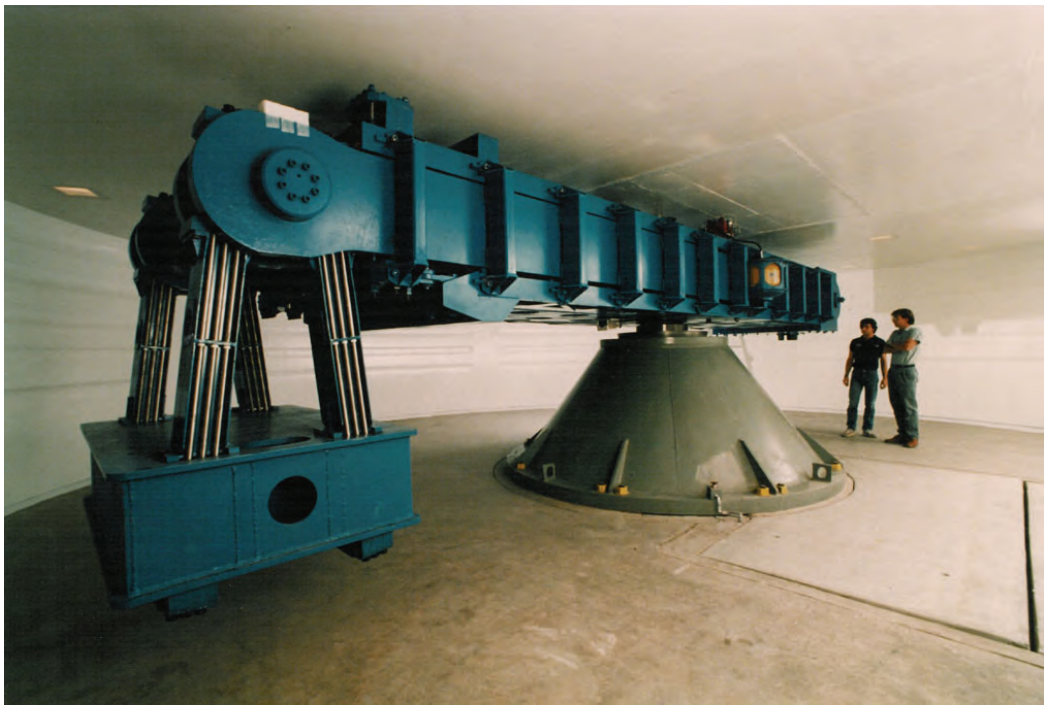

Figure 2.1: Centrifuge at the University of Colorado

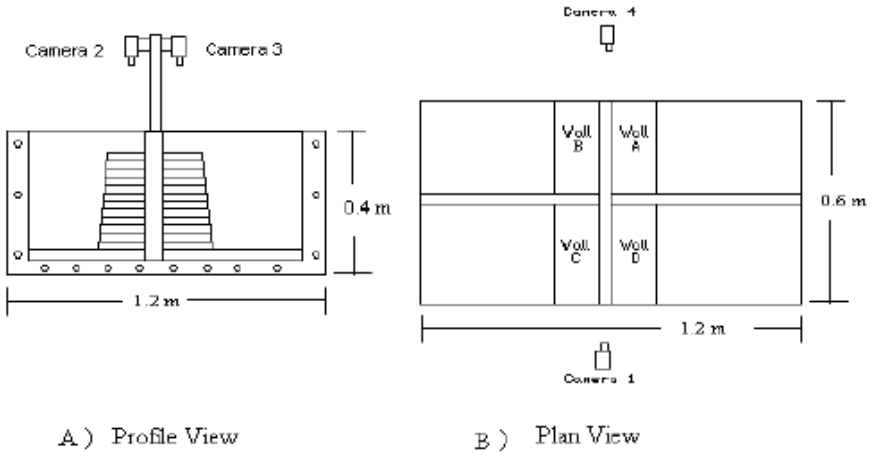

Figure 2.2: A schematic of the testing set up (Woodruff 2003)

2.2.3 Video System

The video system used in the testing program consisted of four cameras mounted to capture an image of each profile and the top of all the models during testing. The pictures captured from cameras can be used to obtain the information of displacement through image processing techniques. This information was analyzed in sequential order to determine the acceleration level at failure and to examine the deformation patterns and the mode of failure. The camera set-up is illustrated in Figure 2.2.

2.3 Material Characteristics

2.3.1 Backfill

Monterey No. 30 sand was used as the backfill material. Monterey No. 30 sand is a poorly graded sand, classified as SP in the Unified Soil Classification Systems (USCU). The gradation curve for Monterey No. 30 is uniform and is illustrated in Figure 2.3.

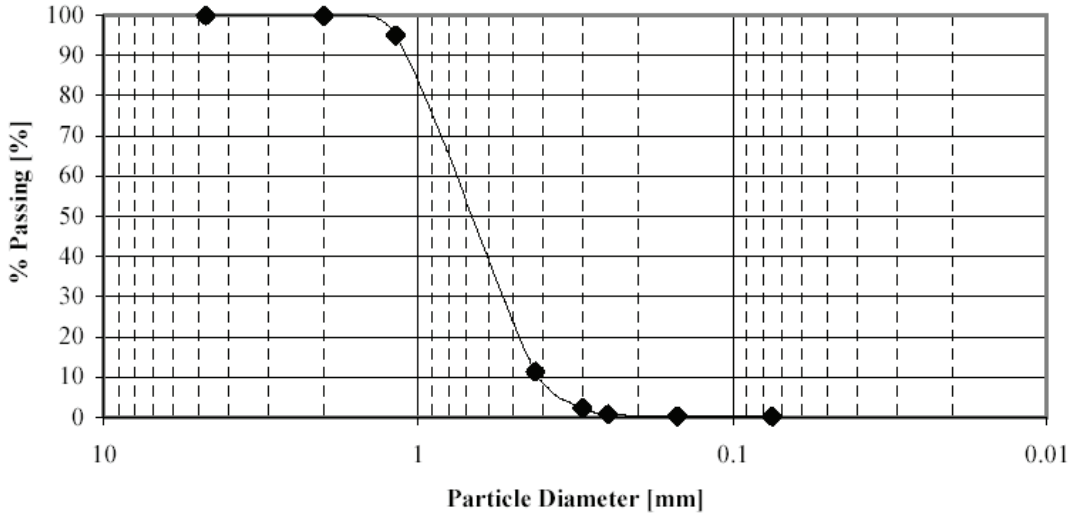

Figure 2.3: Particle size distribution for Monterey No. 30 sand (Arriaga 2003)

The target backfill relative density of 70 percent was reached by pluviating the sand from a height of 120 mm. The Corresponding density is 16.05 kN/m^3. The shear strength values were defined through a series of triaxial tests. The deviatoric stress strain curve of the sand in triaxial compression test can be seen in Figure 2.4. The peak friction angle for Monterey No.30 sand for a relative density of 70 percent is estimated to be 37.7^o. Using correlations reported by Marachi et al. (1981), plane strain friction angle converted from peak friction angle is around 42.2^o.

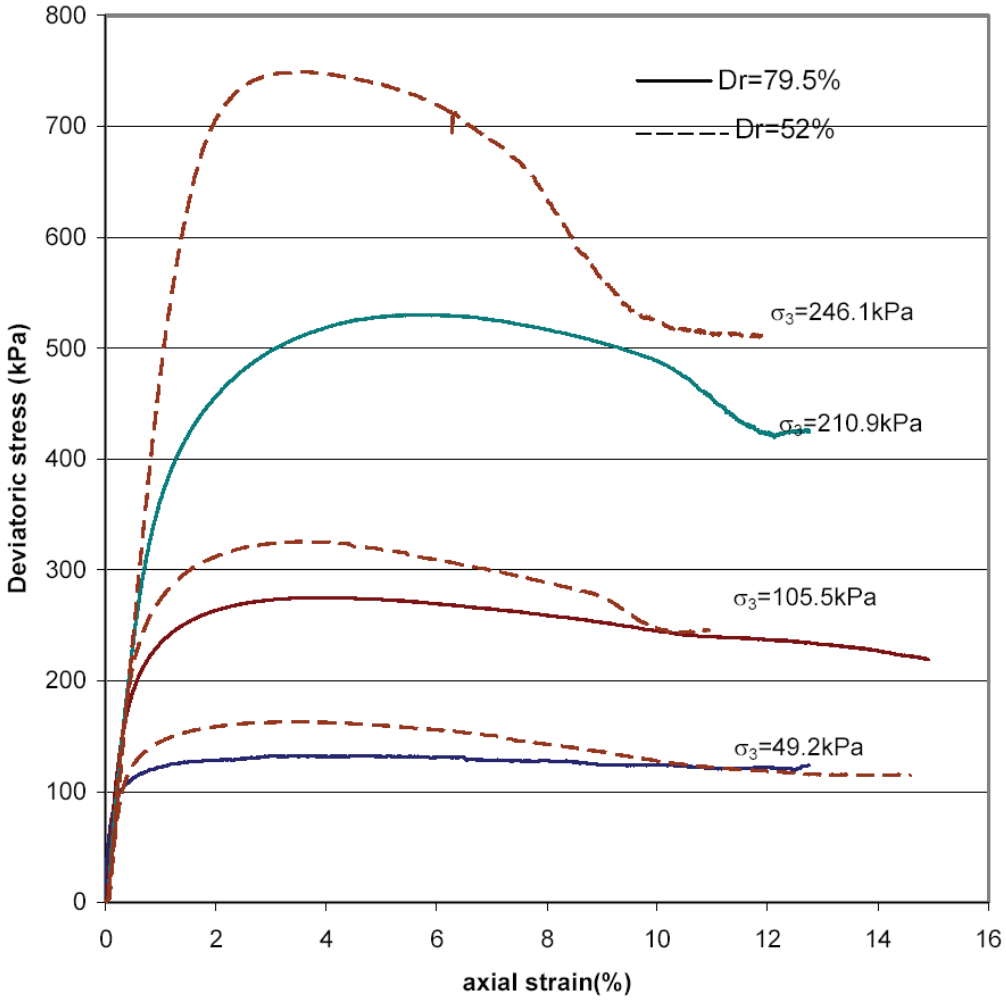

Figure 2.4: Stress-strain curve of Monterey No. 30 sand (Woodruff 2003)

2.3.2 Reinforcements

Two nonwoven geotextiles were used as the reinforcements in this study. The stronger reinforcement, Pellon true-grid, is a white 60 percent polyester, 40 percent rayon fabric with mass per unit area of 28 g/m^2. The weaker reinforcement, Pellon Sew-in, is a white 100 percent polyester fabric with a unit weight of 24.5 g/m^2. A picture of Pellon true-grid is showed in Figure 2.5

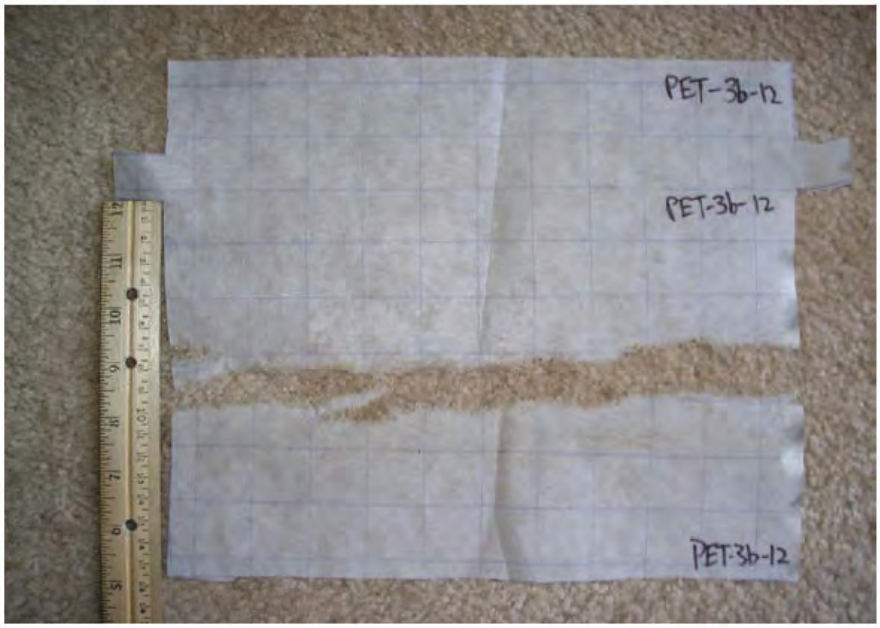

Figure 2.5: Pellon true-grid retrieved after centrifuge testing (Woodruff 2003)

The tensile strength of the reinforcements obtained by wide width strip tensile tests (ASTM D4595) in machine (strong) and transverse (weak) direction are summarized in Table 2.2. Figure 2.6 shows the results of an average wide-width test for the two reinforcements tested in weak direction.

Table 2.2: Unconfined tensile strength of reinforcements (Woodruff 2003)

Geotextile	Direction	Unconfined Tensile Strength (kN/m)	Reinforcement Designations
Pellon Sew-In	Weak Direction	0.03	R1
	Strong Direction	0.1	R3
Pellon True-Grid	Weak Direction	0.09	R2
	Strong Direction	1.12	R4

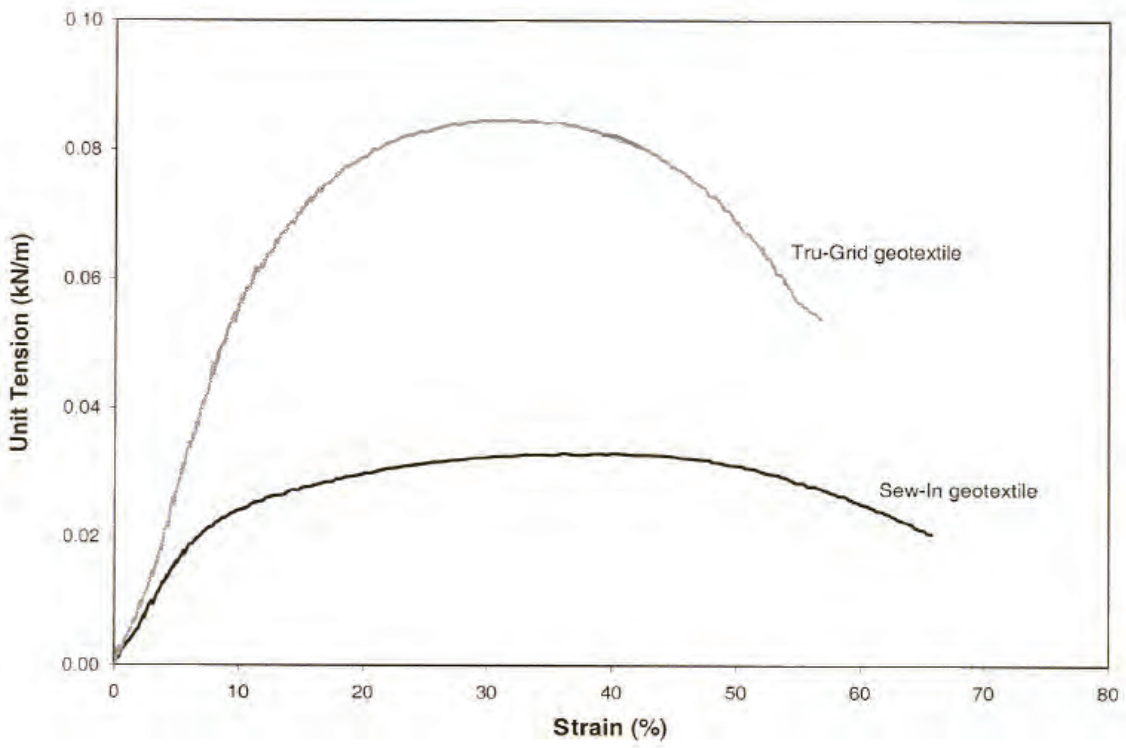

Figure 2.6: Test results from a wide-width tensile test (Woodruff 2003)

Woodruff (2003) performed limit equilibrium analyses to back-calculate the confined tensile strength of reinforcements. He reported the average ratio between the confined tensile strength and unconfined tensile strength to be approximately 2.5. The effect of confined tensile strength will be considered in the finite element and limit equilibrium analyses performed as part of this study.

2.4 Scope of the Testing Program

Woodruff (2003) tested twenty-four different walls with reinforcement lengths (wall widths) ranging from 0.17 to 0.9 times the wall height. All the reduced-scale walls were 230 mm tall and the wall face batter was 11 vertical to 1 horizontal. Wall facing was prepared by wrapping the reinforcement around to retain the backfill. A summary of all tests is listed in Table 2.3.

Table 2.3: Summary of test scope (Woodruff, 2003)

Test		Reinforcement Length	Reinforcement Strength	Reinforcement Configuration at Shoring Interface	Shoring Interface	Vertical Spacing (mm)
1	a	0.9H	R1	Unconnected	Retained Fill	20
	b	0.6H	R1	Unconnected	Aluminum	20
2	a	0.6H	R2	Unconnected	Aluminum	20
	b	0.4H	R2	Unconnected	Aluminum	20
3	a	0.7H	R2	Unconnected	Aluminum	20
	b	0.7H	R2	Unconnected	Retained Fill	20
	c	0.7H	R2	Unconnected	Smooth	20
	d	0.7H	R2	Unconnected	Rough	20
4	a	0.7H	R4	Unconnected	Aluminum	20
	b	0.5H	R4	Unconnected	Aluminum	20
	c	0.3H	R4	Unconnected	Aluminum	20
	d	0.3H	R4	Unconnected	Aluminum	20
5	a	0.17H	R4	Unconnected	Aluminum	20
	b	0.2H	R4	Wrapped Around	Aluminum	20
	c	0.25H	R4	Unconnected	Aluminum	20
	d	0.2H	R4	Wrapped Around	Aluminum	20
6	a	0.3H	R4	Top layer attached	Aluminum	20
	b	0.3H	R4	Top layer wrapped around	Aluminum	20
	c	0.2H-0.3H	R4	Unconnected	Inclined	20
	d	0.3H	R4	Unconnected	Retained Fill	20
7	a	0.25H	R4	Unconnected	Aluminum	10
	b	0.25H	R4	Unconnected	Aluminum	30
	c	0.25H	R4	Unconnected	Aluminum	40
	d	0.25H	R4	Unconnected	Aluminum	50

The tests were grouped into seven main series, which focused on the analyses of the following variables:

- Aspect ratio of the wall
- Reinforcement strength
- Shoring interface
- Reinforcement configuration at the shoring wall interface
- Reinforcement vertical spacing
- Shoring wall inclination

2.5 Results

The walls were loaded to failure. The load (acceleration "g" force) required to fail the wall was recorded. The pictures in Figure 2.7 show a sequence observed in one of these tests (Test 2b), which was subjected to increased gravitational forces until failure occurred. Figure 2.7(c) shows that significant settlement has occurred at the back side of the wall. A “trench” can be observed at the interface between the reinforced backfill and stable wall. This trench tended to pull the MSE wall away from the stable wall, resulting in the collapse of the wall. Horizontal lines (colored sand) shown in the pictures indicate the location of the geosynthetic reinforcements.

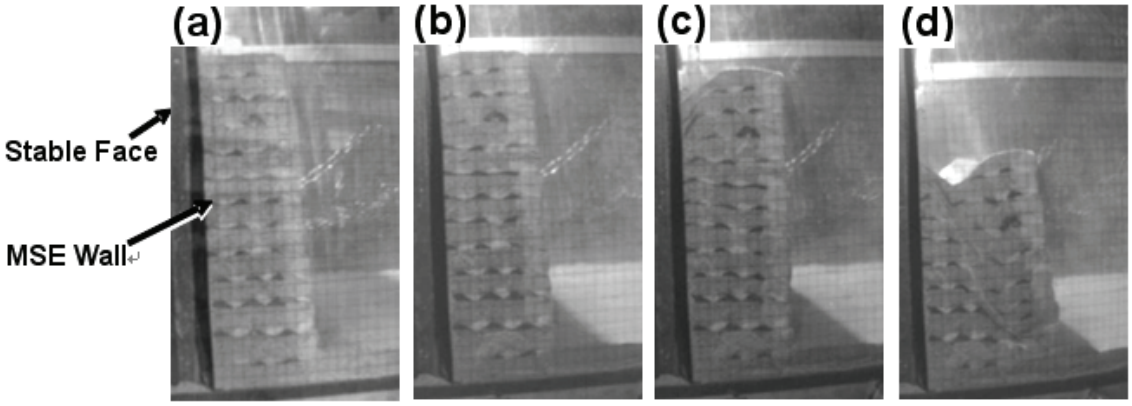

Figure 2.7: Photographic images from centrifuge: (a) Initial condition (gravity); (b) Working Stresses (10g); (c) Before Failure (41g); (d) Failure condition (41g) (Woodruff, 2003)

Three failure modes were reported from observation of the twenty-four tests.

- The first failure mode involves an internal failure. The failure surface goes entirely through the reinforced soil zone. The location of the actual failure surface could be determined based on observed tears (rupture) in each layer of reinforcement.
- The second failure mode involves a compound failure. The failure surface develops partially through the reinforced soil and partially along the interface between the reinforced soil and stable face. Figure 2.8 shows an example of compound failure from Test 2b. The upper four layers of reinforcement were not intercepted by the failure surface and breakage occurred at the lower layers of reinforcement.
- A third failure mode involves an externally overturning failure, where failure surface does not intersect any reinforcement.

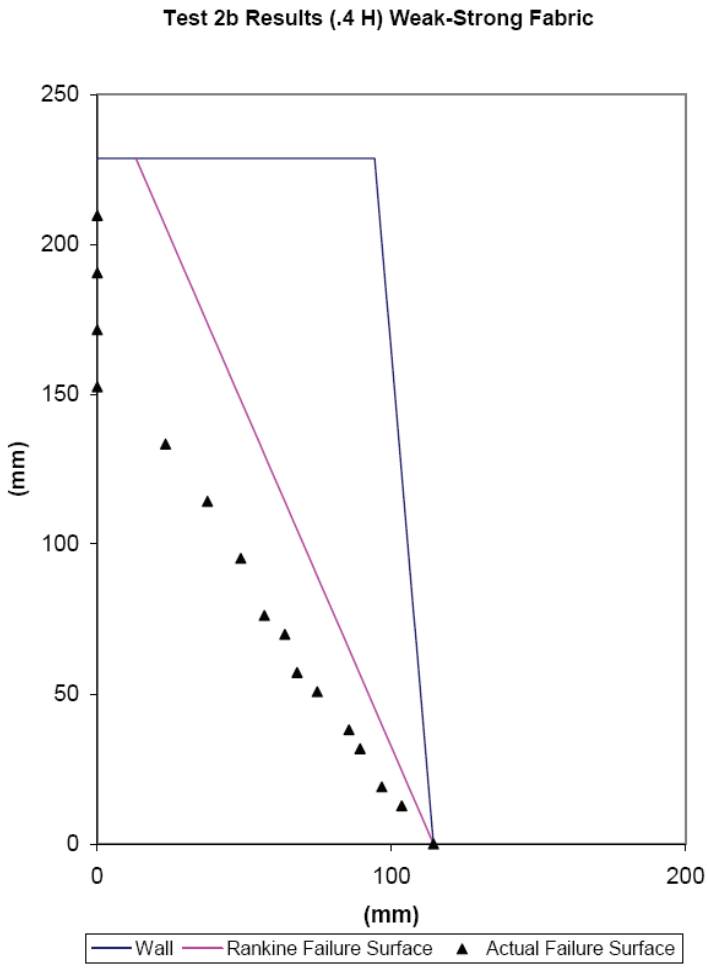

Figure 2.8: An example of compound failure at Test 2b (Woodruff, 2003)

A summary of the g levels at failure and failure modes of all centrifuge tests is listed in Table 2. 4

Table 2.4: A summary of the test results (Woodruff, 2003)

Test		Reinforcement Length	Failure Mode	g-level at failure	g-level at pull away	Vertical Spacing (mm)
1	a	0.9H	Internal	18	None	20
	b	0.6H	Compound	17	17	20
2	a	0.6H	Compound	39	27	20
	b	0.4H	Compound	41	39	20
3	a	0.7H	Internal	38	None	20
	b	0.7H	Internal	49	None	20
	c	0.7H	Internal	47	None	20
	d	0.7H	Internal	44	None	20
4	a	0.7H	None	None	None	20
	b	0.5H	None	None	None	20
	c	0.3H	None	None	22	20
	d	0.3H	None	None	32	20
5	a	0.17H	Overturning	7	5	20
	b	0.2H	None	None	None	20
	c	0.25H	Overturning	32	13	20
	d	0.2H	None	None	None	20
6	a	0.3H	None	None	27	20
	b	0.3H	None	None	30	20
	c	0.2H-0.3H	Overturning	78	25	20
	d	0.3H	None	None	None	20
7	a	0.25H	Overturning	38	31	10
	b	0.25H	Overturning	2.5	1	30
	c	0.25H	Overlap Pullout	1	None	40
	d	0.25H	Overlap Pullout	1	None	50

2.6 Conclusions

The main conclusions drawn from this study with regard to each of the variables are as follows:

- **Aspect ratio of the wall:**
  Walls with aspect ratios larger than 0.6 failed in an internal failure mode. Walls with aspect ratios equal or less than 0.6 failed in a compound failure mode. Externally overturning failure mode typically resulted when the wall aspect ratio was reduced below 0.25.

- **Reinforcement strength:**
  Test series 1 through 3 failed internally due to the use of reinforcements with comparatively low tensile strength. Stronger reinforcements in test series 4 through 7 effectively prevented internal failure due to the breakage; however, the failure mode would switch to the external failure or no failure occurred until the completion of test. No failure of model walls occurred when extra design considerations were implemented to prevent the external failure; for example, test 6a: attached top layer to stabilized wall and test 6b: wrapped around the top layers of reinforcements in the back side close to the shored wall,

- **Shoring interface:**
  The roughness of the shoring interface was investigated; however, in Test series 3, the results of the effect of interfacial roughness on the stability of model walls didn't have a clear trend.

- **Reinforcement configuration at the shoring wall interface :**
  Wrapping around the back reinforcement layer showed that the wall was stable up to very high acceleration levels. This suggests that the failure mode changes due to the wrapping around configuration. Attaching the top reinforcement appears to add stability to the wall.

- **Reinforcement vertical spacing:**
  Decreasing the spacing of the reinforcement was observed to increase the stability of the walls with very short aspect ratios, suggesting that close reinforcement spacing reduces lateral earth pressures.

- **Shoring wall inclination:**
  Inclined shoring systems appeared to stabilize the wall due to the longer reinforcement lengths at the top of the wall and the longer moment arm to resist the overturning moments.

Other important observations were made from the centrifuge tests. First, the failure planes have an inclination less than the theoretical Rankine failure plane when a shoring wall is present. However, the walls in front of a retained fill have a failure surface close to the theoretical Rankine failure surface. Second, when the wall aspect ratio decreased below 0.3, the failure mode changed from internal/ compound failure to external failure. Woodruff (2003) reported that the external failure initiated from a "trench" at the interface between the reinforced backfill and stable wall and this trench had a tendency to pull MSE wall away from the stable wall resulting in external failure.

3. Finite Element Analysis

3.1 Finite Element Model

The finite element program Plaxis version 8.2 (Plaxis, 2005) was used to conduct the numerical analysis in this study. Finite element simulations were performed to model centrifuge tests 2b and 5c. Test 2b was compared to centrifuge test in detail under both working stress and failure conditions. This comparison would be treated as a verification of the suitability of the finite element model. Test 2b was also used to study the development of a "trench", which was observed from centrifuge tests as a premonitory symptom of failure. Test 5c was used as a part of parametric study to understand the effect of the trench as a function of the wall aspect ratio.

3.1.1 Initial Geometry and Boundary Condition

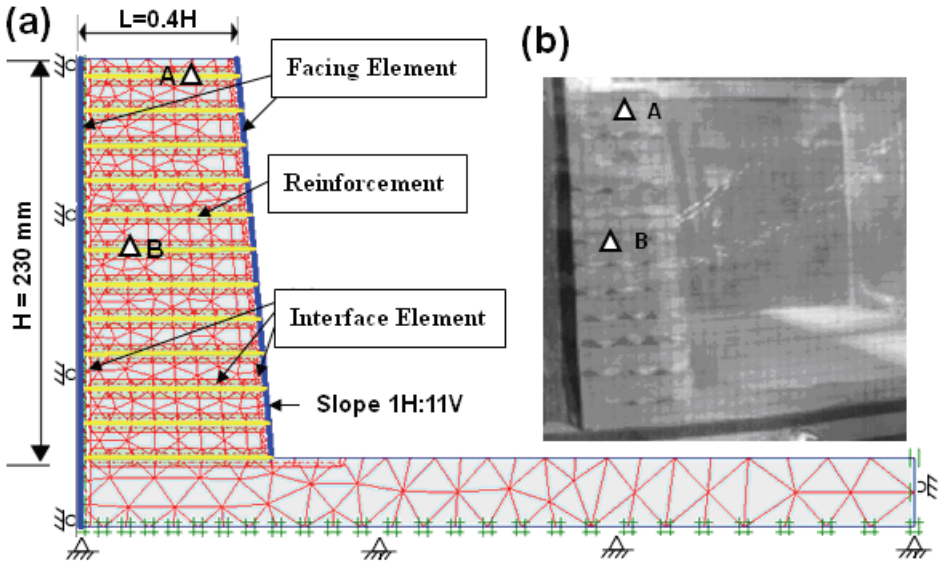

Figure 3.1: Wall geometry of Test 2b: (a) Finite element setup and initial mesh; (b) Picture from centrifuge at initial condition

Figure 3.1(a) shows the mesh used to simulate centrifuge test 2b. Figure 3.1(b) shows the initial condition of centrifuge test 2b. The finite element meshes are composed of 15-node isoparametric triangular elements. The mesh coarseness was set as "Fine", which would generate around 500 triangular elements for a given geometry. Horizontal fixities (rollers) were applied to the stable face. This allowed the wall to settle in the vertical direction but prevented the nodes along the boundary from moving laterally. Total fixities were placed at the bottom of the foundation. Plane strain was assumed. Staged construction was simulated by conducting layer-by layer construction in Plaxis. The centrifugal force of the centrifuge was simulated by increasing

the unit weight (body force) on the wall. This technique allows the simulation to follow a realistic loading path and to produce representative. In conventional modeling technique, the effect of centrifugal force was modeling by rescaling the dimensions of the reduced wall into prototype dimensions. Updated mesh analysis was activated to take into account the effect of large deformation, especially important at failure condition.

3.1.2 Backfill Model and Material Properties

The backfill soil material used in the centrifuge was Monterey No. 30 sand. The Hardening Soil model (Plaxis, 2005) was selected to simulate the nonlinear elastic response. The Hardening Soil model is a stress-dependent hyperbolic model based on the flow rule and plasticity theory. The Hardening Soil model was expected to have better ability to match the stress-stain curves of granular soil at working stress conditions than the Mohr-Coulomb model, a linear elastic and perfect plastic model. The angle of dilatancy (ψ) was used to account for the dilatation of sand during shearing. The value was calculated by the empirical equation $\psi \approx \phi - 30°$ (Bolton ,1986). Another important aspect was the sensitivity of the soil properties to relative density. Therefore, three triaxial compression tests with specimen relative density 65 percent (close to density 70 percent reported in centrifuge tests) were used to calibrate the backfill parameters. Figure 3.2 shows the result of the calibration of the Hardening Soil model. The parameters of the Hardening Soil model are listed in Table 3.1.

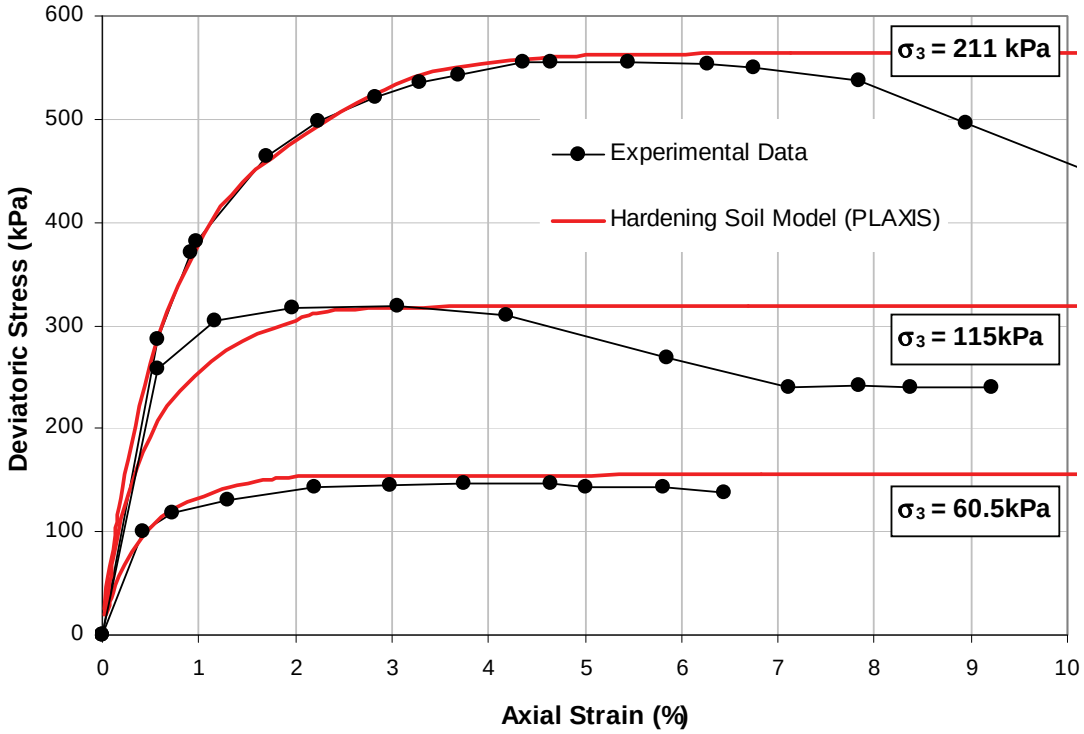

Figure 3.2: Stress-strain curves for drained triaxial tests on Monterey #30 sand

Table 3.1: Material properties for sand backfill

Bulk unit weight of backfill	**Value**
γ (unit weight) (kN/m^3)	16.05
Strenght properties	
ϕ (peak friction angle) (degrees)	36.7
c (cohesion) (kPa)	5 (1)
ψ (angle of dilatancy) (degrees)	6.7
Stiffness properties (Hardening Soil model)	
E_{50}^{ref} (secant stiffness) (kPa)	35000
E_{ur}^{ref} (unloading/reloading stiffness) (kPa)	105000 (2)
E_{ode}^{ref} (tangent stiffiness for primary odeometer loading) (kPa)	60000
m (modulus exponent)	0.5
R_f (failure ratio)	0.85
u_{ur} (Poisson's ratio for unloading/reloading)	0.2

Note: (1) Cohesion was set a small value for numerical purpose

(2) E_{ur}^{ref} was assumed to be $3E_{50}^{ref}$ as the default value in Plaxis

3.1.3 Reinforcement and Facing Elements and Material Properties

The reinforcements were modeled as line elements with a normal stiffness but with no bending stiffness. Line elements could only sustain tensile forces but no compression. An elastoplastic model was selected to mimic breakage of the reinforcement. The input parameters for the reinforcements were the elastic axial stiffness EA and ultimate axial tensile strength, N_p. The value of EA was determined as the secant modulus at 2 percent strain from the wide width tensile tests. The value of N_p was adopted from the peak strength of the wide width tensile test. The value of EA and N_p were multiplied by an average back-calculated strength ratio to account for the differences between unconfined and confined geotextile conditions. The value of the average back-calculated strength ratio is 2.5, as reported by Woodruff (2003). A summary of reinforcement parameters are listed in Table 3.2

Table 3.2: Material properties for reinforcement and facing elements

Reinforcement	Value
R2 (weak direction)	
EA (axial stiffness) (kN/m)	1.25
N_p (maximum tensile strength) (kN/m)	0.0225
R4 (strong direction)	
EA (axial stiffness) (kN/m)	1.4
N_p (maximum tensile strength) (kN/m)	0.025
Facing elements	
Wall face (geotextile-wrap around)	
EI (bending stiffness) (kNm^2/m)	1.2
EA(bending stiffness) (kN/m)	502
Stable face (Aluminum)	
EI (bending stiffness) (kNm^2/m)	10000
EA(bending stiffness) (kN/m)	10000

Plate elements were used to represent the stabilized and MSE wall faces. Plates are structural objects composed of beam elements with bending stiffness, EI, and normal stiffness, EA. The values of EI and EA for the stable face were set high enough to prevent compression and deflection in the plate. A parametric study was performed to find the appropriate input values for a flexible wall face, geotextile wrapped around face in the case of centrifuge tests. The values of normalized EI and EA were decreased to reduce the rigidity of the facing element, and the final values of normalized EI and EA were selected by the criteria of the earth pressure along the wall face, no longer decreasing with the decrease of normalized EI and EA values. A detailed discussion on the selection of normalized input values, as well as an example of calculation is presented in Appendix A. The facing parameters are also listed in Table 3.2

3.1.4 Interface Models and Material Properties

The study in the companion report (Kniss et al., 2007) successfully captured the reduction of earth pressure due to the arching effect by employing interface elements. In this study, interface elements were introduced adjacent to the wall face, stable face, and reinforcement elements to reproduce the soil-structure interaction. The material properties of an interface element correspond with backfill properties; however, the strength of the interface can be controlled by an interface reduction factor, R_{inter}. The value of R_{inter} depended on the roughness of the surface; A R_{inter} of 1/3 was assigned to the soil-stable face (aluminum) interface elements and 9/10 to the soil-wall face (geotextile) and soil-reinforcement (geotextile) elements.

3.2 Results

The results of the finite element simulation of Test 2b are compared to the results measured from centrifuge test under working stress and failure conditions. As will be shown in sections 3.2.1 and 3.2.2, these comparisons show that the finite element simulations can capture the behavior of a centrifuge test. The simulation of Test 2b is also used to study the mechanics of

the "trench." The simulation of Test 5c is only used as a parametric study to understand how this trench develops with the decrease of wall aspect ratio.

3.2.1 Working Stress Condition

As previously mentioned, body forces were applied to simulate the centrifugal force. The magnitude of the applied body force is a multiple of gravity. For example, the body force 2g would be equivalent to twice the force applied by gravity. Locations A and B (see Figure 3.1) were selected to track the relative displacements through out applied body forces ranging from 3g to 10g. Because of the centrifuge data not reliable at lower g-levels, the displacement data below 3g was not included. The relative displacements were calculated using distance equation as follows:

$$d = \sqrt{(x_{Ng} - x_{3g})^2 + (y_{Ng} - y_{3g})^2} \qquad \text{Eq.(1)}$$

where:

d is the relative displacement between 3g and Ng;
Ng is any interested g-level;
X_{3g} and Y_{3g} are the coordinate of location A or B at 3g;
X_{Ng} and Y_{Ng} are the coordinate of location A or B at Ng.

The coordinates were determined by importing the camera-recorded images into an image processing program self-developed using Matlab. Figure 3.3 shows the comparisons of results between experimental measurements and measurements from the finite element analysis. The general trends show good agreement at locations A and B. The discrepancies may be the result of error in tracking the selected locations or from the low resolution of the images.

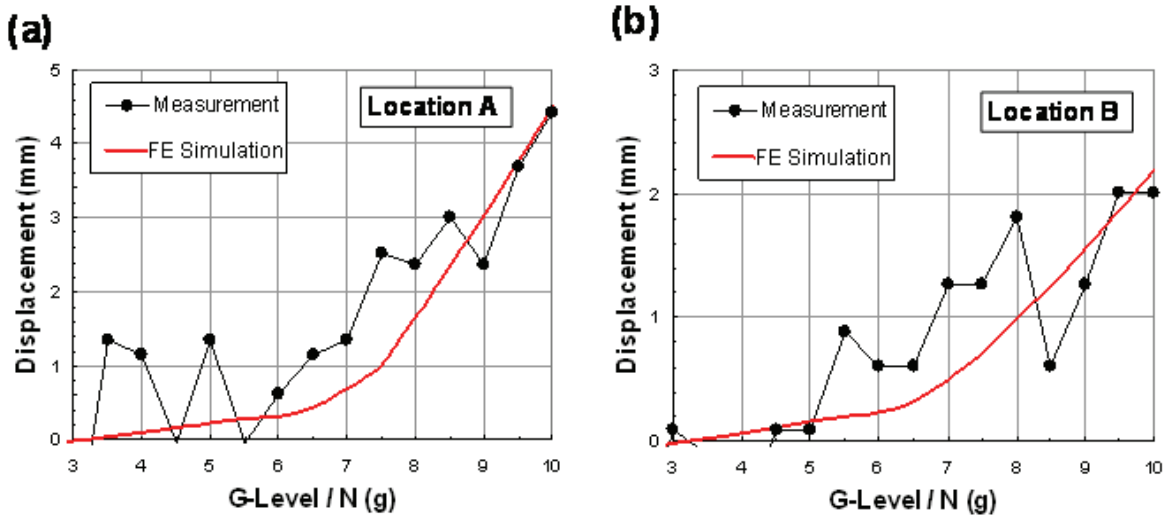

Figure 3.3: Comparison of displacement at working stress condition: (a) Location A; (b) Location B

3.2.2 Failure Condition

After applying a body force equal to 10g, a Phi-C reduction function was selected for the next series of analyses. In Phi-C reduction function, the strength parameters tanϕ and c of the soil were successively reduced until failure of the structure occurs. The strength of the interfaces was also reduced in the same way. The global factor of safety can be obtained by this approach. The factor of safety is defined as ratio of available soil strength to strength at failure. This factor of safety can be used to evaluate the stability of MSE walls.

Failure Characteristics

The failure characteristics observed from the finite element simulation and centrifuge test were compared. In Figure 3.4(a) and (b), the displacement contours produced from the finite element simulation shows a displacement trend that is similar to that obtained from the centrifuge image, obtained immediately before failure. Both the FE simulation and the centrifuge model showed an upper layer wall sliding downward and a triangular part at the bottom of the wall remaining stationary.

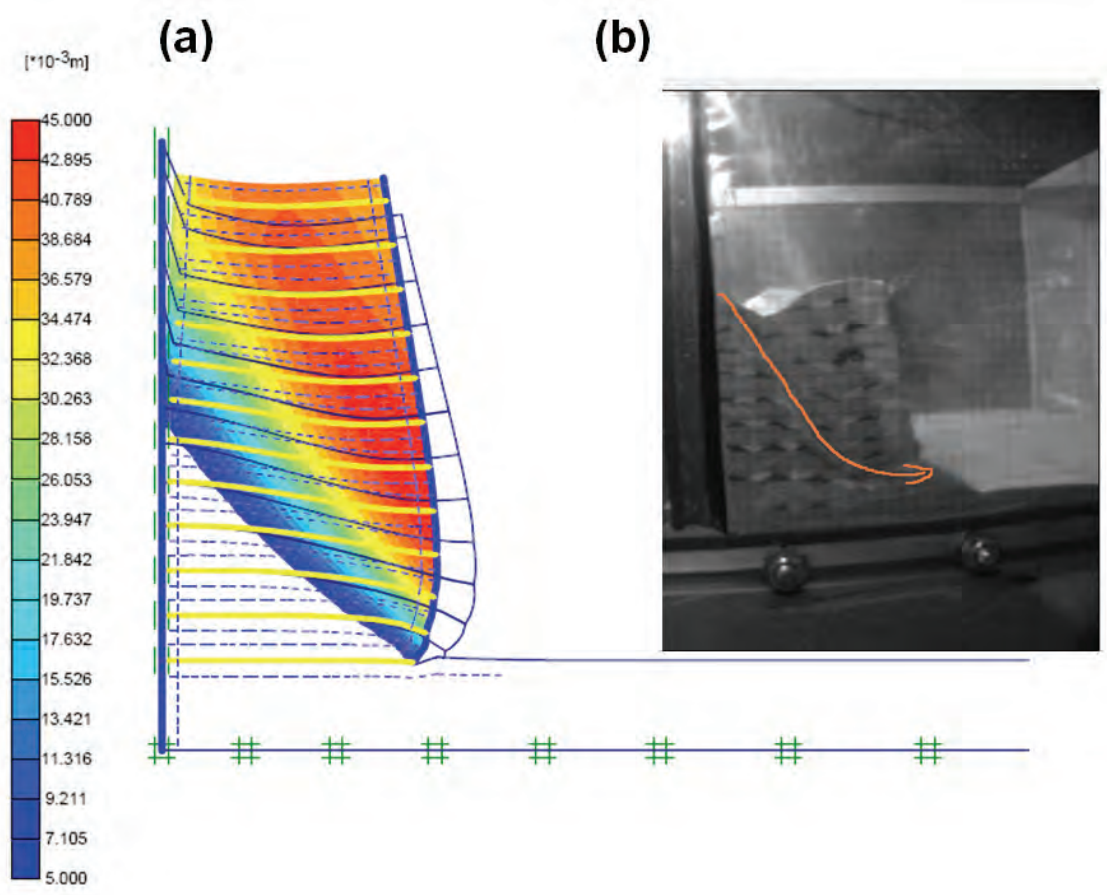

Figure 3.4: Comparison of displacement: (a) displacement contour from finite element simulation; (b) Image from centrifuge.

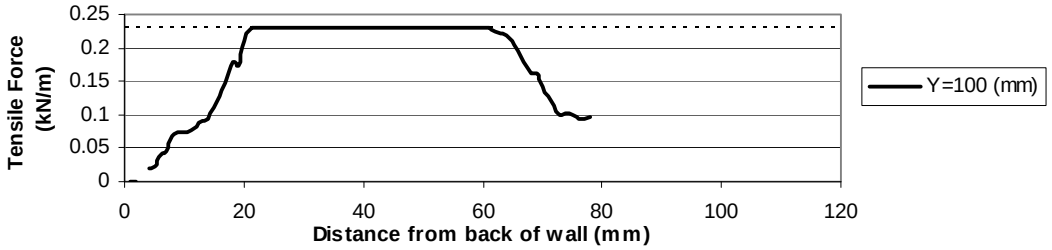
Tensile Force (kN/m)
0.25
0.2
0.15
0.1
0.05
0
0
20
40
60
80
100
120
Distance from back of wall (mm)
Y=100 (mm)

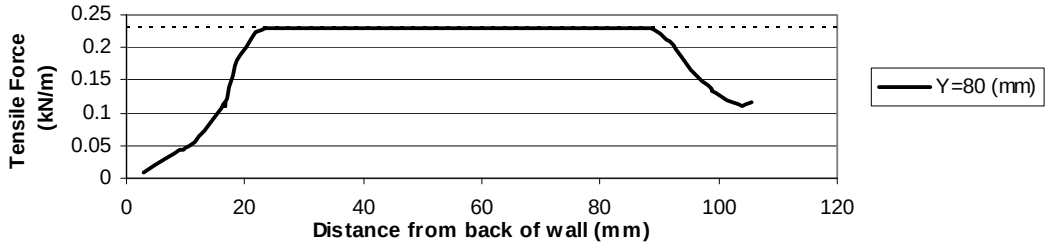
Tensile Force (kN/m)
0.25
0.2
0.15
0.1
0.05
0
0
20
40
60
80
100
120
Distance from back of wall (mm)
Y=80 (mm)

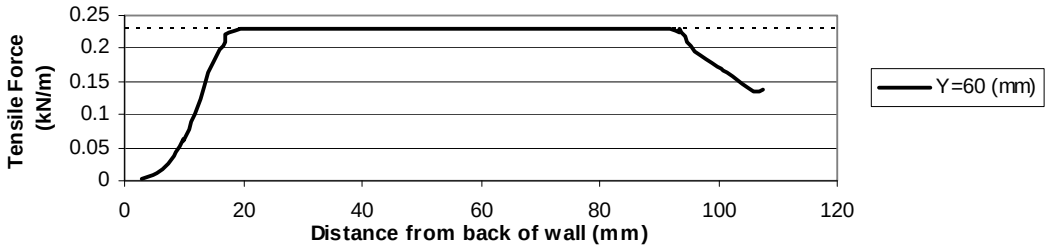
Tensile Force (kN/m)
0.25
0.2
0.15
0.1
0.05
0
0
20
40
60
80
100
120
Distance from back of wall (mm)
Y=60 (mm)

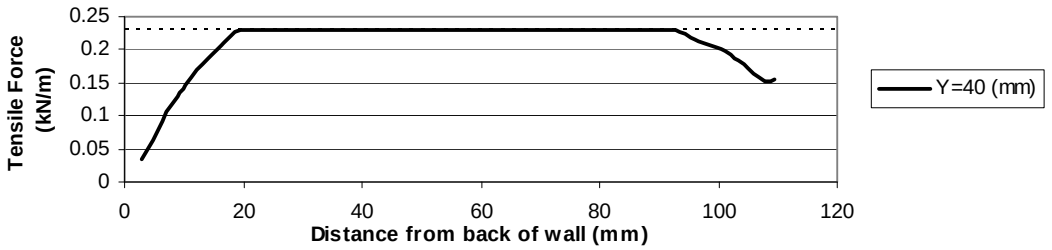
Tensile Force (kN/m)
0.25
0.2
0.15
0.1
0.05
0
0
20
40
60
80
100
120
Distance from back of wall (mm)
Y=40 (mm)

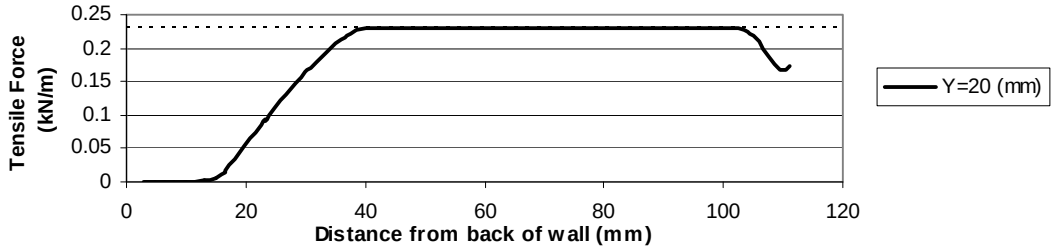
Tensile Force (kN/m)
0.25
0.2
0.15
0.1
0.05
0
0
20
40
60
80
100
120
Distance from back of wall (mm)
Y=20 (mm)

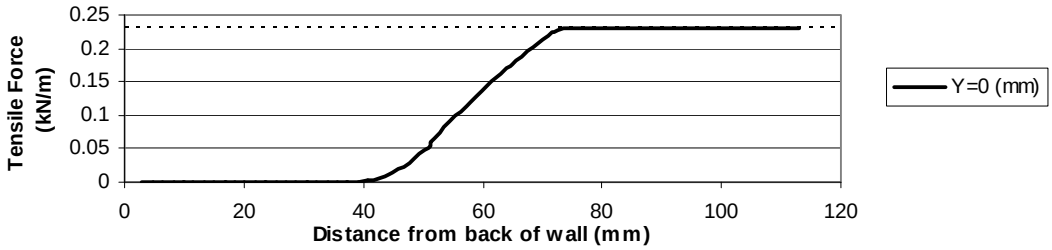
Tensile Force (kN/m)
0.25
0.2
0.15
0.1
0.05
0
0
20
40
60
80
100
120
Distance from back of wall (mm)
Y=0 (mm)

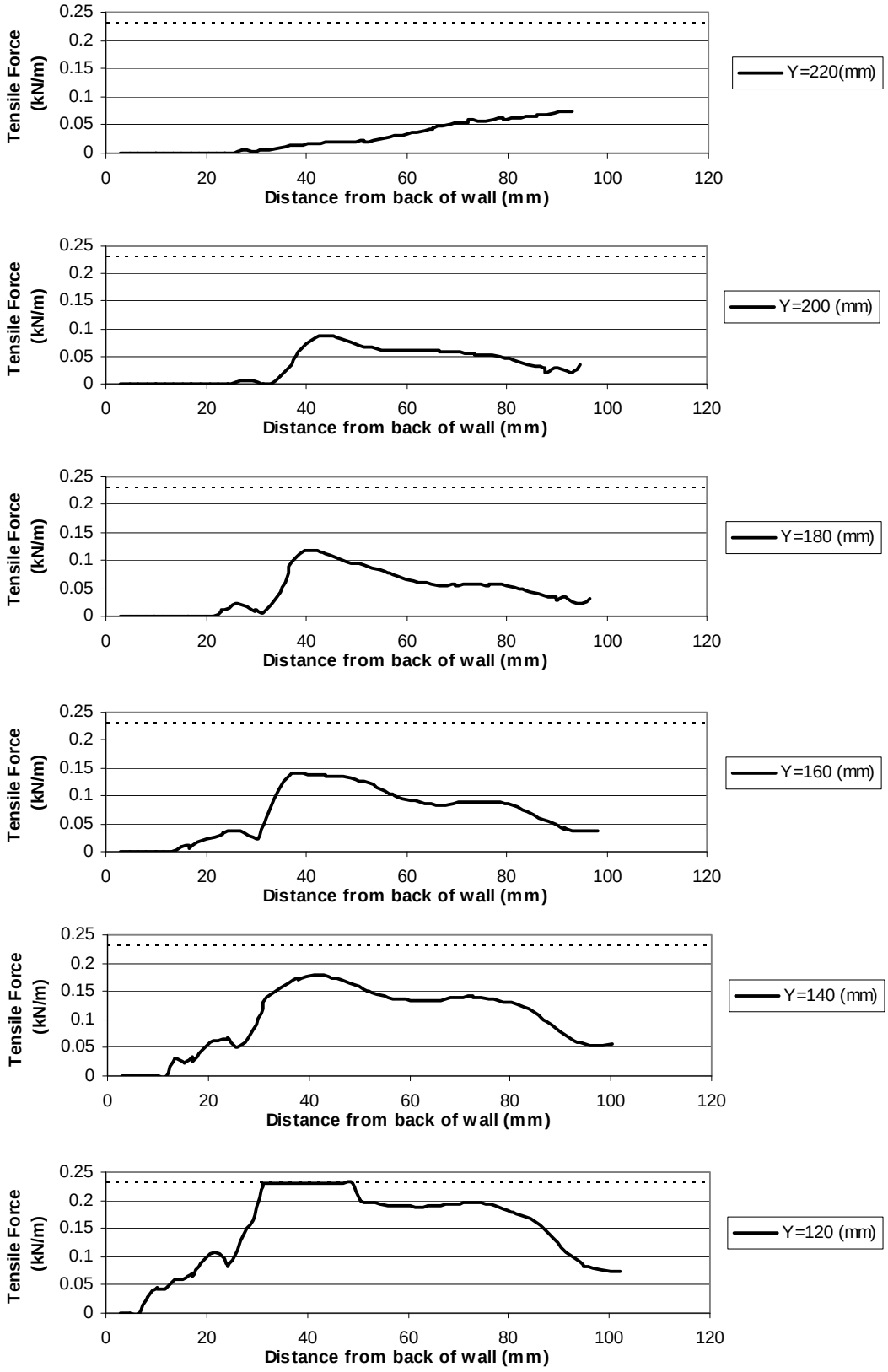

Figure 3.5: Development of tensile force along each layer of reinforcements

Development of Tensile Forces in the Reinforcements

As shown in Figure 2.8 and Table 2.4, the failure mode of Test 2b involves a compound failure. This compound failure can also be reproduced in a finite element simulation. Figure 3.5 shows the tensile force developed along each layer of reinforcements. Dash lines in Figure 3.5 represent the input value of ultimate tension strength, N_p. The maximum tensile force reaching ultimate tensile strength (input value) corresponds to breakage of the reinforcements (at lower layers from Y=0 to 120 mm); a tensile force less than the ultimate strength means breakage of reinforcement did not occur (at upper layers from Y=140 to 220 mm). Figure 3.6(a) shows a summary of maximum tensile force at each reinforcement layer and Figure 3.6(b) shows the actual reinforcements after the centrifuge test. In Figure 3.6(b), the experimental results showed that the lower eight layer reinforcements broke and the upper four layers did not. Consequently, it may be concluded that experimental results support the FE simulation results.

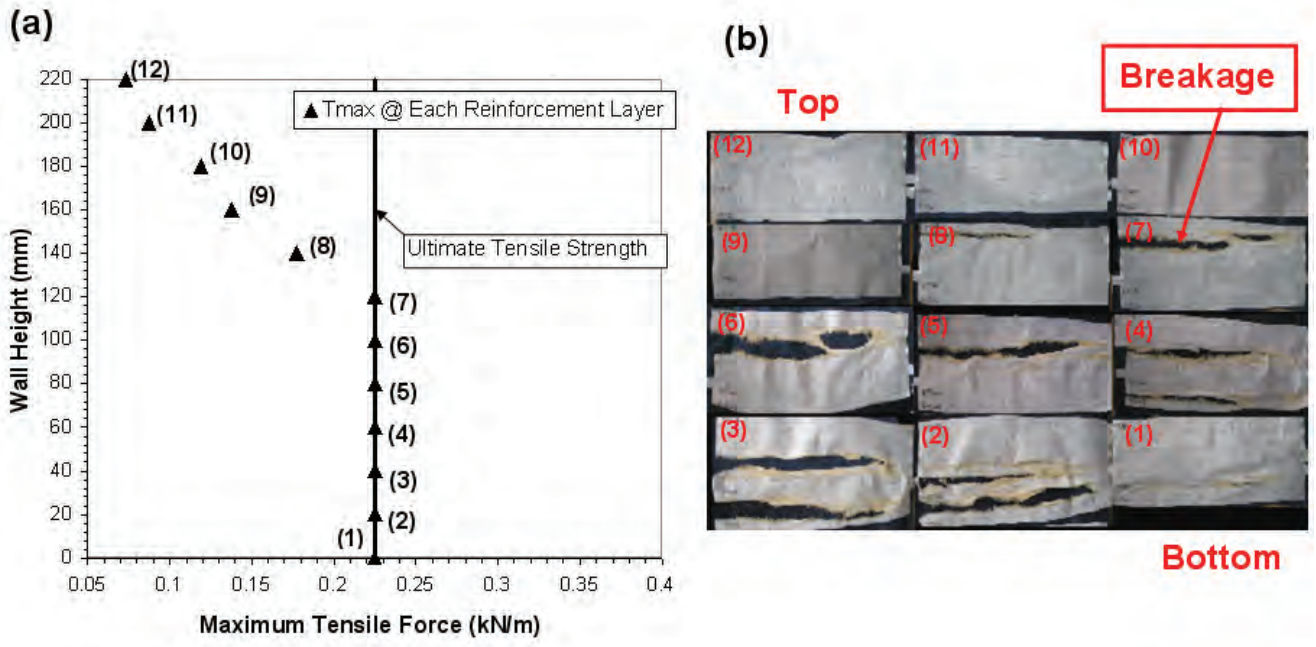

Figure 3.6: Comparison of breakage of reinforcements: (a) Results from finite element simulation; (b) Image of reinforcement.

3.2.3 Development of a Zero Pressure Zone at the Interface

The normal stress acting along the interface between the wall and the stable face was examined to monitor the formation and mechanics of the development of a trench. The interface element has zero thickness; therefore, the normal stress acting on the interface is identical to that acting on the stable face. A tensile strength of interface equal to 1 kN/m (default is zero) was assigned as a property of this interface. This allows Plaxis to generate the tensile points around certain areas, which are subjected to tension instead of compression.

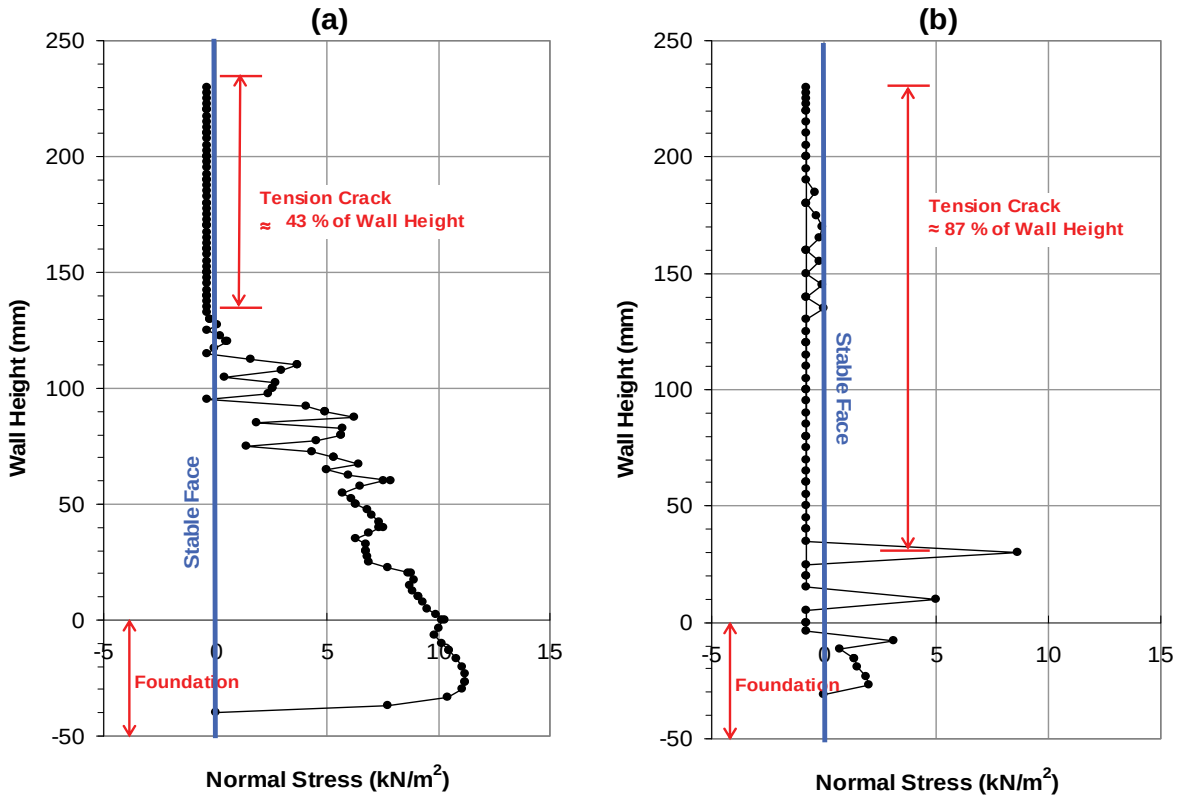

Figure 3.7: Distribution of normal stress along interface face: (a) Test 2b; (b) Test 5c.

Figure 3.7(a) shows the distribution of normal stresses along the interface for Test 2b. Positive normal stress represents compression while negative stress represents tension. The results in Figure 3.7(a) suggest that the trench observed by Woodruff corresponds to a tension zone. The tension results numerically from assuming a small cohesion for the soil constitutive model done to avoid numerical instabilities. Besides, the existence of tension in sand or gravel material is unrealistic, so the results from this finite element simulation should be interpreted as the development of a zero pressure/normal stress zone along interface between the soil and stable face. This could cause the backfill material to settle into the crack, as observed from centrifuge tests [see Figure 2.7(c)], leading to redistribution of stresses and ultimately the instability and failure of the wall.

In Test 2b, a zero pressure zone initiated along the interface between the wall and stable face and extended to a depth of approximately 0.43H for the wall with aspect ratio 0.4. Test 5c was also analyzed to understand how the zero pressure zone develops with decreasing wall aspect ratio. The procedure of simulating Test 5c is consistent with that of Test 2b. Figure 3.7(b) shows the distribution of normal stresses along the interface for Test 5c. Comparing Test 2b and Test 5c, this zone increased from around 43 percent to 87 percent of the wall height as wall aspect ratio decreases from 0.4 to 0.25. It may be expected the length of this zone could reach entire wall height at wall aspect ratio 0.25, regardless of few spikes showing positive normal stresses around the bottom portion of the wall.

3.3 Lessons Learned from Finite Element Simulations

Because of experimental difficulties associated with the use of pressure cells, the centrifuge modeling can only reveal information about displacements and deformations of the walls. Yet, the stress distribution is important to understand the failure mechanism. Fortunately, this information can be obtained from properly calibrated finite element simulations. Figure 3.8 shows information on the stresses from the finite element simulation of Test 2b at the moment of failure. The plastic points in Figure 3.8 correspond to the stresses of soil at that point is beyond the elastic region into the plastic region. Plastic points represent failure of soil at that point. The tension points shown in Figure 3.8 correspond to soil regions under tension instead of compression.

Based on Figure 3.8, the following considerations are listed (see corresponding number in Figure 3.8):

1. **Eliminate tension at the interface:**

   Possible solutions include attaching reinforcements to the stable face, extending upper reinforcements over the existing wall, and wrapping around the top layers of reinforcements in the side of close to shored wall.

2. **Limit large deformations of the front face:**

   Possible solutions include using rigid face (e.g., concrete panel or block) rather than flexible face (e.g., geosynthetics wrap around).

3. **Decrease the number of plastic points in the wall:**

   Possible solution involves increasing strength of backfill, i.e., high strength backfill or high compaction effort, or increasing the function of reinforcement.

4. **Minimize plastic points in the foundation:**

   Figure 3.8 shows the plastic points would spread to the foundation. Methods of improving the strength of foundation could be adopted.

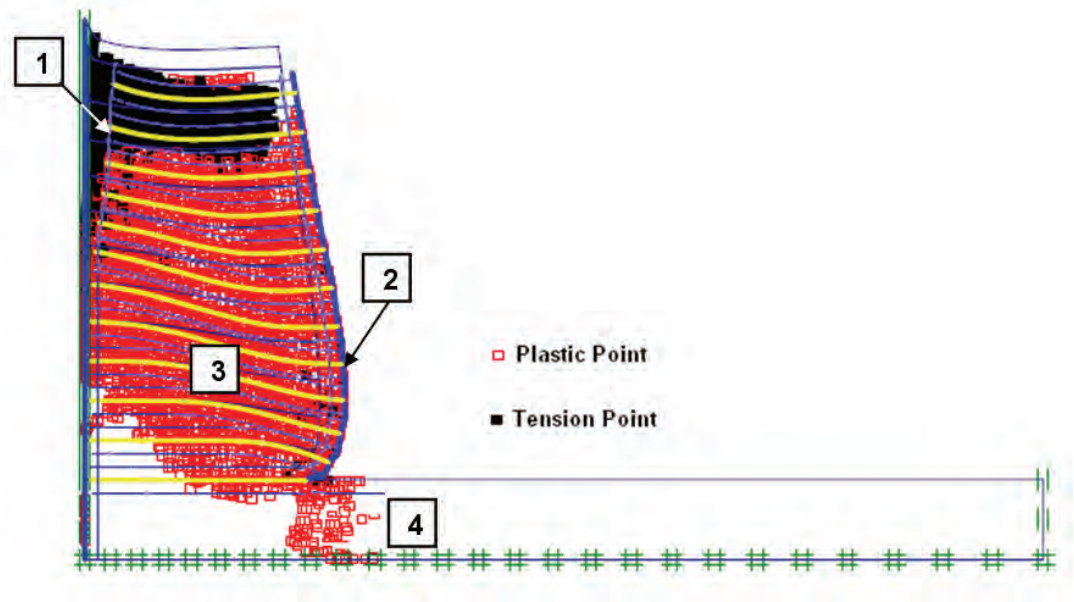

Figure 3.8: Stress points of Test 2b at failure condition

3.4 Conclusions

This chapter presented a finite element simulation of centrifuge models, conducted to better understand the behavior and mechanics of narrow MSE walls. The results predicted by the finite element model were compared to the results from centrifuge test under working stress and failure conditions. Experimental and numerical results matched well. The validated model used in this study could serve for designing narrow MSW walls of specific configurations being considered for implementation by TxDOT.

Interpretation of the stress information showed that the failure of narrow MSE wall was triggered by a zero pressure zone located in the vicinity of the interface between stable and MSE walls. This zone extends further below the crest as the wall width became narrower and reaches approximately the bottom of wall for aspect ratios below 0.25. As a result of this zero pressure zone, the backfill tends to sink into the crack and ultimately cause failure of the wall.

Design considerations were identified to improve the stability of the wall by obviating the development of a zero pressure zone. They include eliminating tension at the interface, limiting large deformations of the front face, decreasing the number of plastic points in the wall, and minimizing plastic points in the foundation. Future study should focus on the evaluation of the proposed design considerations.

4. Limit Equilibrium Analysis

4.1 Limit Equilibrium Approach

The analyses presented in this chapter were conducted using limit equilibrium. The UTEXAS4 program developed by Dr. Stephen Wright at The University of Texas at Austin (Wright 1999) was used. The primary reason for using limit equilibrium analyses in addition to the finite element analyses is that limit equilibrium methods are mostly used in geotechnical engineering practice to evaluate the stability of MSE walls and their ability to accurately predict failure mechanisms.

In this chapter, the limit equilibrium method was used to model three centrifuge tests: Test 2a (L/H=0.6), Test 2b (L/H=0.4) and Test 3a (L/H=0.7). Because similar procedures were followed in the three tests, only the description of mode Test 2b is discussed in detail in Section 4.1. Further, the results obtained from limit equilibrium analyses are compared with centrifuge tests to verify use of the proposed limit equilibrium model. A parametric study was also performed to investigate the effect of the reinforcement actual tension as well as the effect of using inputted reinforcement strength recommended in FHWA design guidelines. Finally, a design chart defining inclination angles as a function of various wall aspect ratios was developed. The engineers can use this chart to find the location of failure surface and calculate the factor of safety against pullout.

4.1.1 Modeling of Wall Systems

Figure 4.1 shows the wall geometry of Test 2b, with a wall height of 230 mm, wall aspect ratio of 0.4 at top of the wall, wall face batter 11 vertical to 1 horizontal, and twelve layers of reinforcement (20 mm vertical spacing). Two methods have been used to simulate the effect of centrifugal force. First, the effect of centrifugal force can be simulated by increasing the body force on the wall model. This can be achieved by multiplying unit weight of backfill by N times corresponding to the target g-level. Second, the effect of centrifugal force can be simulated by rescaling the dimensions of the test wall. This can be achieved by enlarging wall dimensions N times corresponding to the target g-level. The first method was adopted in this simulation because this technique avoids re-drawing wall geometry every time g-level is increased. The modeling of backfill, reinforcements and the method of searching noncircular failure surface are discussed in Sections 4.1.2, 4.1.3, and 4.1.4.

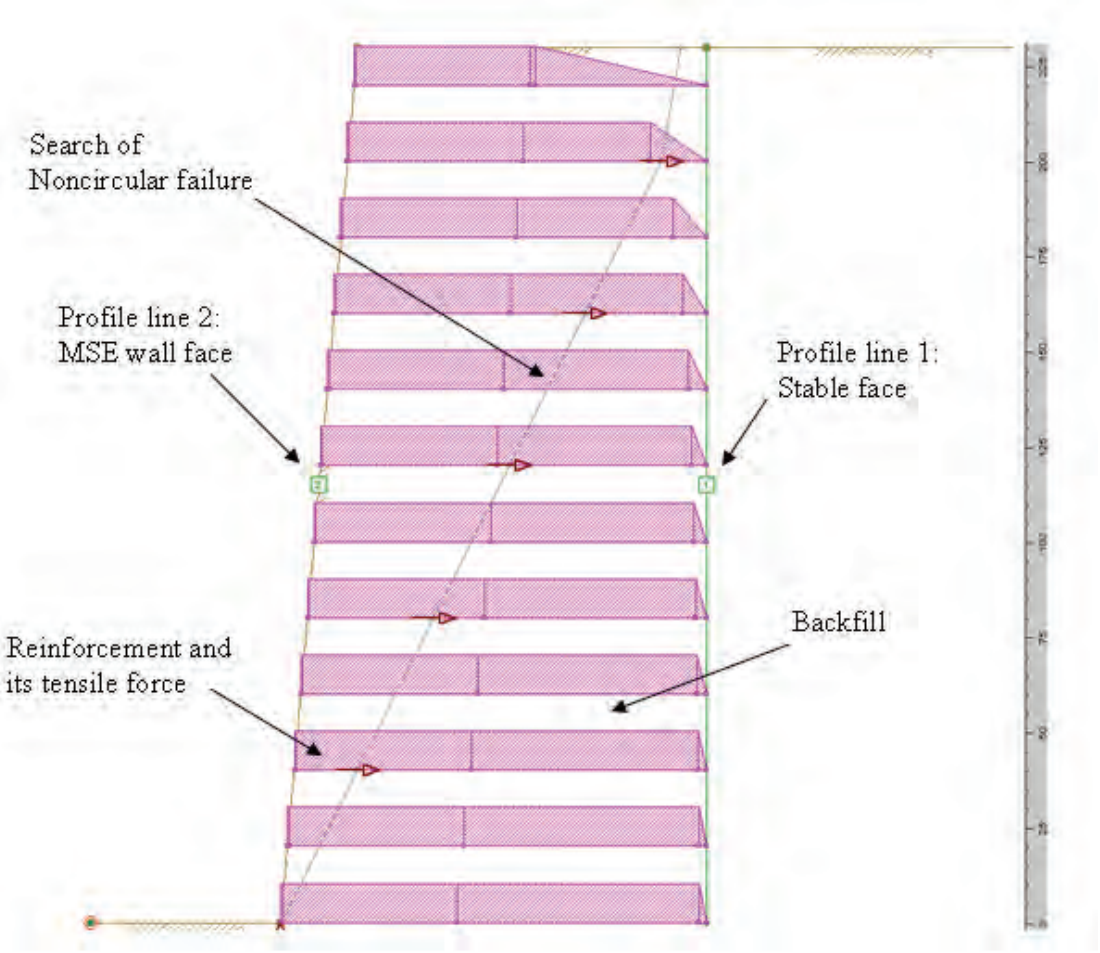

Figure 4.1: Wall model of Test 2b

4.1.2 Modeling of Backfill in MSE and Stable Wall

The Stable wall (wall behind stable face) was assigned a material modeled with infinite strength (very strong material) and unit weight of 25 kN/m^3. Because the existing wall is assumed stable, the infinite strength of the stabilized wall precludes failure surfaces passing through the stable face and constrain the search of the critical slip surface only within the MSE wall.

Material model of the backfill in MSE wall was selected following a conventional Mohr-Coulomb model. Monterey No. 30 sand with relative density of 70 was characterized by unit weight of 16.05 kN/m^3, plane strain friction angle of 42.2º and zero cohesion. The centrifugal force was simulated by increasing the unit weight of backfill by N times corresponding to the target g-level; for example, the unit weight 658.05 kN/m^3 (=16.05*41) for the modeling of centrifugal force at 41g.

4.1.3 Modeling of Reinforcement

The forces in the reinforcement are limited by its ability to resist failure by rupture and by pullout (See Figure 4.2). The ways of modeling rupture and pullout resistance of the reinforcement are discussed below.

Tensile Forces

For the limit equilibrium analyses, the resistance of the reinforcement against failure by rupture was assumed to be the same for all layers of reinforcement, i.e., the same reinforcing material was assumed to be used in each layer. Wide width strip tensile tests (ASTM D4595) showed the unconfined tensile strength of reinforcements used in Test2b was 0.09 kN/m. In order to evaluate the confined tensile strength of the reinforcement, Woodruff back-calculated the confined tensile strength for each centrifuge tests by force equilibrium analysis. The average confined tensile strength reported based on this analysis was 2.5 times larger than the unconfined tensile strength of reinforcements. Consequently, a confined tensile force 0.225 kN/m (=0.09*2.5) was used as the tensile strength in each layer of reinforcements.

Pullout Resistance

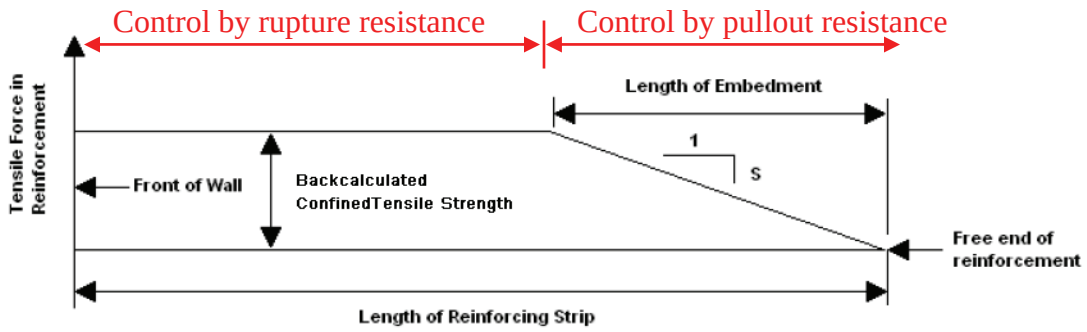

Figure 4.2: Schematic of assumed distribution of tensile stresses in the reinforcement

The pullout resistance of the reinforcement was assumed to increase linearly from zero at the free end of the reinforcement to a value equal to the tensile strength of the reinforcement. Figure 4-2 illustrates the variation of the longitudinal force in the reinforcement. The rate of change in force with horizontal distance, shown as S in Figure 4-2, can be evaluated by Equation 4.1, which was derived based on FHWA design guidelines.

$$S = F^{*} C R_c \alpha_v \sigma_{ov} \qquad \text{Eq.(4.1)}$$

where:

F^* is the pullout resistance factor,
C is the reinforcement effective unit perimeter,
R_c is the coverage ratio,
α_v is a scale correction factor which accounts for non-linear stress reduction,
σ_{ov} is the vertical overburden stress acting on the reinforcement,

The recommended equation for the pullout resistance factor (F^*) for geosynthetic reinforcement is defined in the current FHWA design guidelines for MSE walls (Elias et al, 2001) as follows:

$$F^* = \frac{2}{3}\tan\phi' \qquad \text{Eq. (4.2)}$$

Based on this recommendation and a friction angle (ϕ') of 42.2°, the value of F^* was adopted as 0.60. The effective unit perimeter of the reinforcement (C) was assigned a value of 2 to account for the top and bottom face of the reinforcements. The coverage ratio (R_c) for geosynthetic reinforcement is 1 because the reinforcement is a uniform sheet of material. The value of α_v was assigned as 1.0. σ_{ov} is the vertical overburden stress acting on the reinforcement.

In a condition for narrow walls, where the aspect ratio is low, several studies have showed arching effect will reduce the vertical and horizontal earth pressures. This arching effect was included in the limit equilibrium calculations by evaluating $\sigma_{ov,}$ as follows:

$$\sigma_{ov} = \gamma z \beta_v \qquad \text{Eq. (4.3)}$$

where:

γ is the unit weight of the reinforced backfill,
z is the depth of the layer of reinforcement below the top of the backfill,
β_v is the vertical stress influence factor

The companion report (Kniss et al., 2007) conducted a series of finite element simulations to study the effect of arching effect on the vertical and horizontal stresses. The values of vertical stress influence factors (β_v) varying with wall aspect ratios proposed are shown in Figure 4.3.

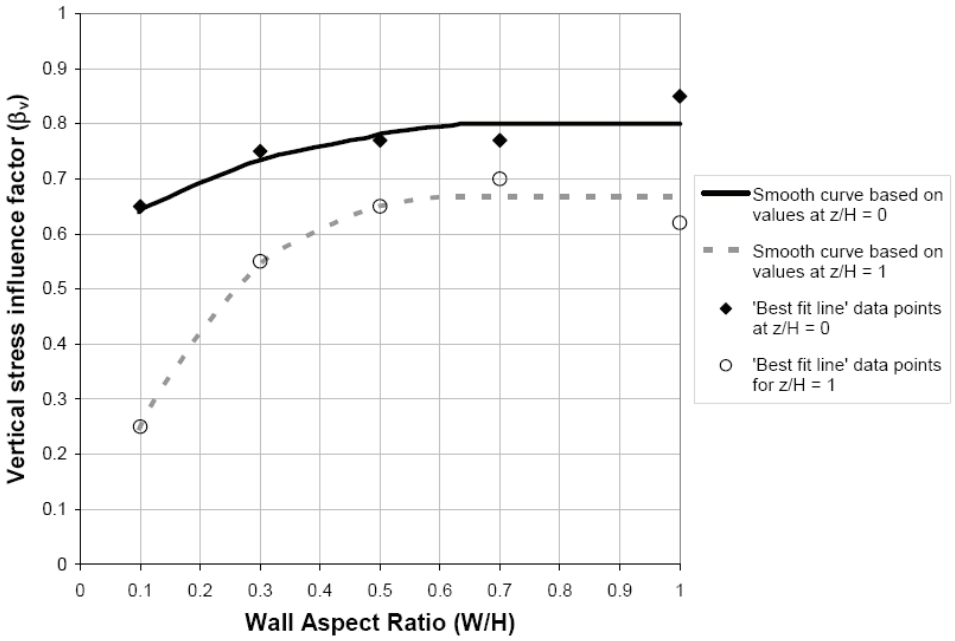

Figure 4.3: Values of the vertical stress influence factors at the top and bottom of the wall plotted as a function of the wall aspect ratio (Kniss 2007)

For the case of wall aspect ratio 0.4 in Test 2b, a value of 0.65 was selected based on Figure 4.3 to represent the average value of vertical stress influence factor between top and bottom layers. The final distribution of tensile forces of the reinforcements is shown in Figure 4.1.

Overlap Layer of Reinforcement

The experimental results from the centrifuge models showed that the overlapping reinforcement layers increased the stability of the system. Consequently, the contribution of the geotextile overlap layers to the stability of the models was incorporated in the limit equilibrium models. The tensile force in the overlap layer was modeled using confined tensile force constantly through the entire overlap layer. The length of reinforcement was inputted as 50 mm, which corresponds to the length of the overlap layers in the centrifuge test.

Orientation of Reinforcement Tension

The resistance provided by the reinforcement is characterized in terms of longitudinal and transverse forces at selected points along each layer of the reinforcement. The longitudinal force represents the resistance in the reinforcement parallel to the length of the reinforcement, and the transverse force represents the resistance in the reinforcement perpendicular to the length of the reinforcement. However, it was assumed that the reinforcement only provides resistance in the longitudinal direction and the resistance in the transverse direction was assumed to be zero.

4.1.4 Search for Noncircular Failure Surface

Limit equilibrium calculations were performed using Spencer's method (Spencer 1967). This method satisfies all equilibrium conditions i.e., vertical force, horizontal force, and moment

equilibrium. The interslice forces were assumed to be parallel to each other. This assumption is required to balance the number of unknown parameters and the number of equilibrium equations. Based on the study conducted by the companion report (Kniss et. al, 2007), it was concluded that the noncircular failure surfaces are more critical than circular failure surfaces. Also based on the observation from Woodruff (2003), the critical failure surface of a narrow wall showed a bilinear rather than circular shape. Therefore, limit equilibrium analyses in this study were performed using a search for a noncircular failure surfaces.

The searches for the noncircular failure surfaces were initiated by specifying the initial location of selected points along the failure surface. The companion report (Kniss et. al, 2007) performed a parametric study to find the adequate number of points to define the initial failure surface. The study showed that an initial failure surface defined by from five to nine points is adequate. The seven points, evenly distributed through the height of the wall, were selected to define the initial failure surface. Figure 4.1 shows the location of selected seven points used as an initial failure surface.

In all analyses, the first point on the initial failure surface was fixed at the toe of the wall. The last point was placed at the crest of the MSE wall. Fixing the first point at toe forced the failure surface to pass through this point, but other points on the initial failure surface were only allowed to move horizontally.

4.2 Results

The results of the analyses for the three centrifuge tests are presented in this section. The factor of safety at failure and the location of failure surface are the two most important results obtained from limit equilibrium analysis. In this section, these results are compared to the experimental results from centrifuge testing.

4.2.1 Factor of Safety versus G-Level

Figure 4.4 shows the calculated factor of safety as a function of the g-level for Test 2b (wall aspect ratio 0.4) as obtained using limit equilibrium. The factor of safety decreases with increasing g-level. The figure also shows that the wall is predicted to fail (FS=1) around 42g. Centrifuge testing indicated the wall failed at approximately 41g. Consequently, the g-levels at failure from centrifuge testing and limit equilibrium simulation are in close agreement.

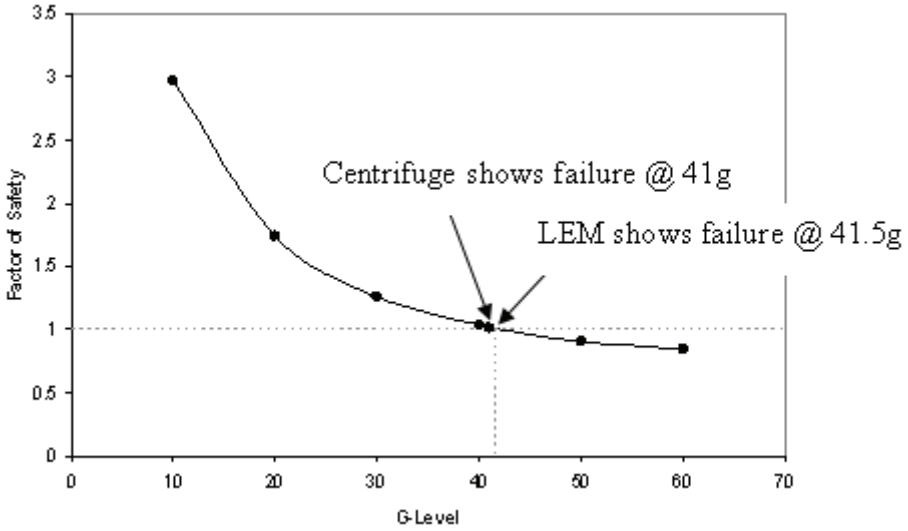

Figure 4.4: Factor of safety versus g-level for Test 2b

Figure 4.5 and Figure 4.6 show the plot of factor of safety versus g-level from the limit equilibrium simulations of Tests 2a and 3a, respectively. Test 2a has a wall aspect ratio of 0.6 and Test 3a has a wall aspect ratio of 0.7. Both simulations show that the wall fails (FS=1) around 38g. Centrifuge tests indicated that the wall failed around 40g. The results of limit equilibrium simulations of Tests 2a and 3a indicate that the g-levels at failure from both centrifuge testing and limit equilibrium simulations are in a good agreement with each other.

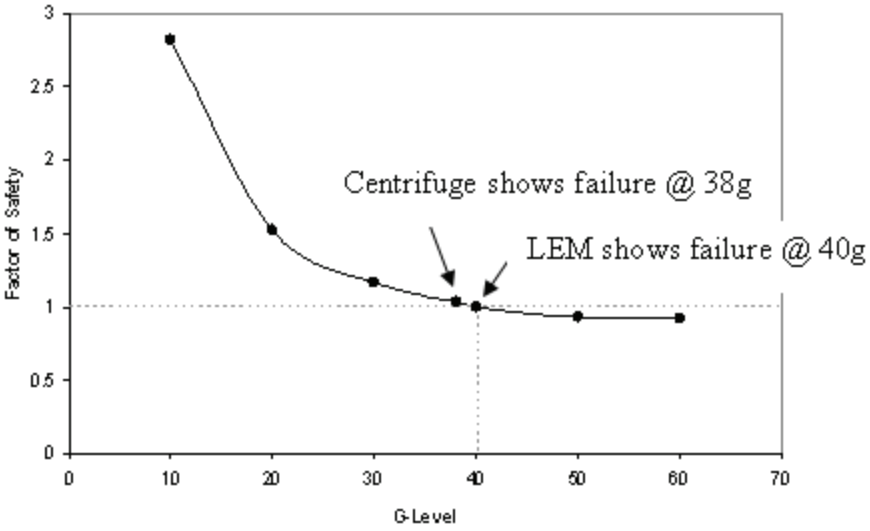

Figure 4.5: Factor of safety versus g-level for Test 2a

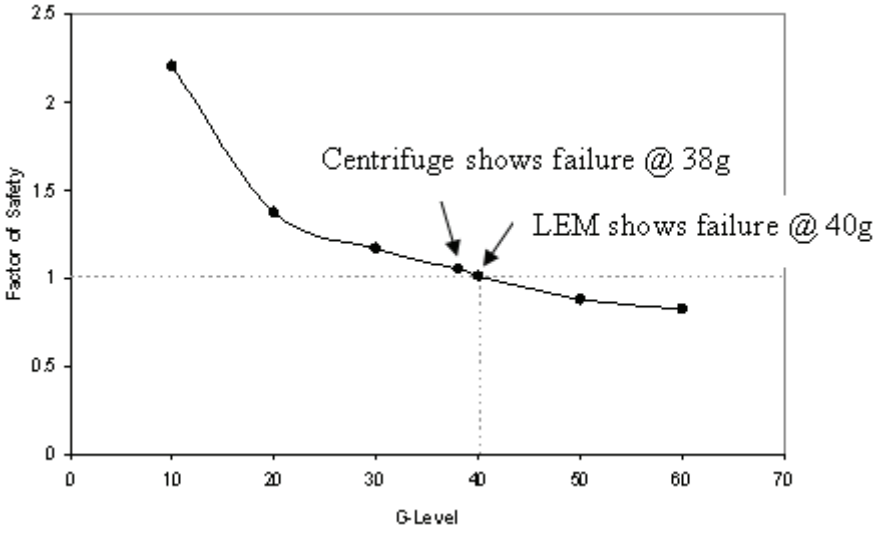

Figure 4.6: Factor of safety versus g-level for Test 3a

4.2.2 Location of the Failure Surface

In reinforced soil structures, the portion of the reinforcement that extends beyond the failure surface provides resistance against pullout. Therefore, location of failure surface is important to determine the pullout resistance of the reinforcement and eventually for the design of these structures. Figure 4.7 shows a comparison between the location of the failure surface obtained experimentally from Test 2b and the one obtained using limit equilibrium analysis. Both the experimental and predicted results show the failure surface goes partially through the reinforced soil and partially along the interface between the reinforced soil and stable face. Finally, the inclination angle of the failure surface is less than the theoretical value defined by the Rankine failure surface criteria.

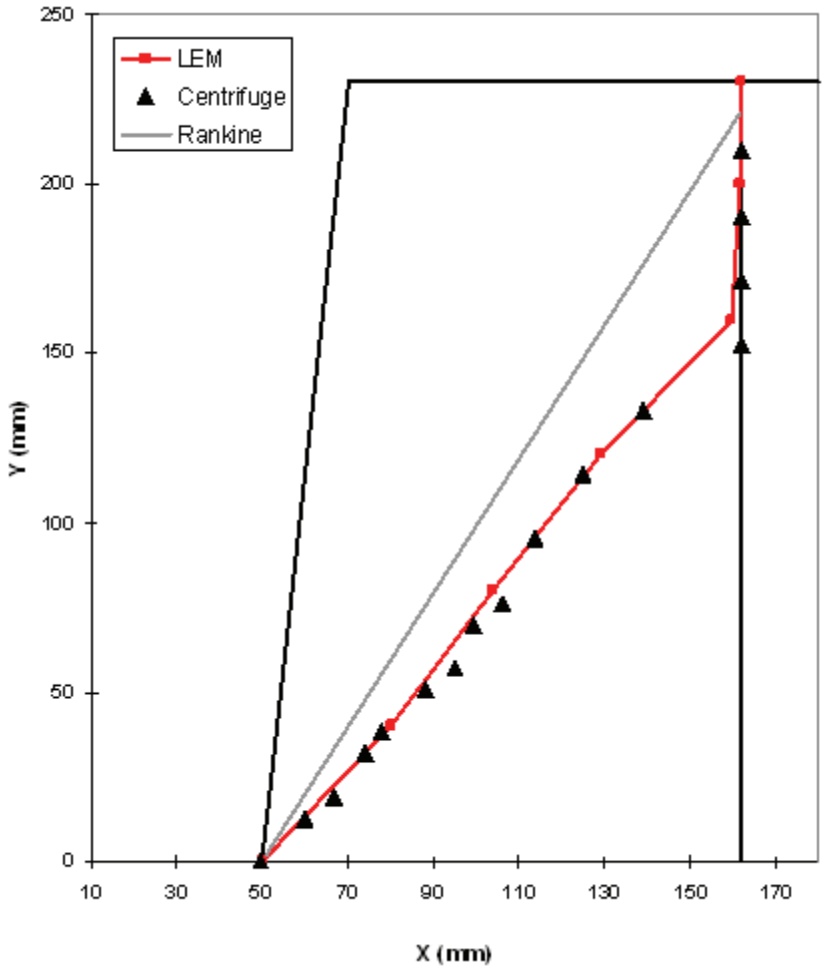

Figure 4.7: Location of failure surface for Test 2b

Figures 4.8 and 4.9 show the comparison between the location of the failure surface obtained experimentally from Test 2a and Test 3a, respectively, and those obtained using limit equilibrium analyses. Good agreement can be observed. The discrepancy only happened at the top of the failure surface in Figure 4.8, as predicted failure surface did not go along the interface near the top of the wall as shown by the experimental results.

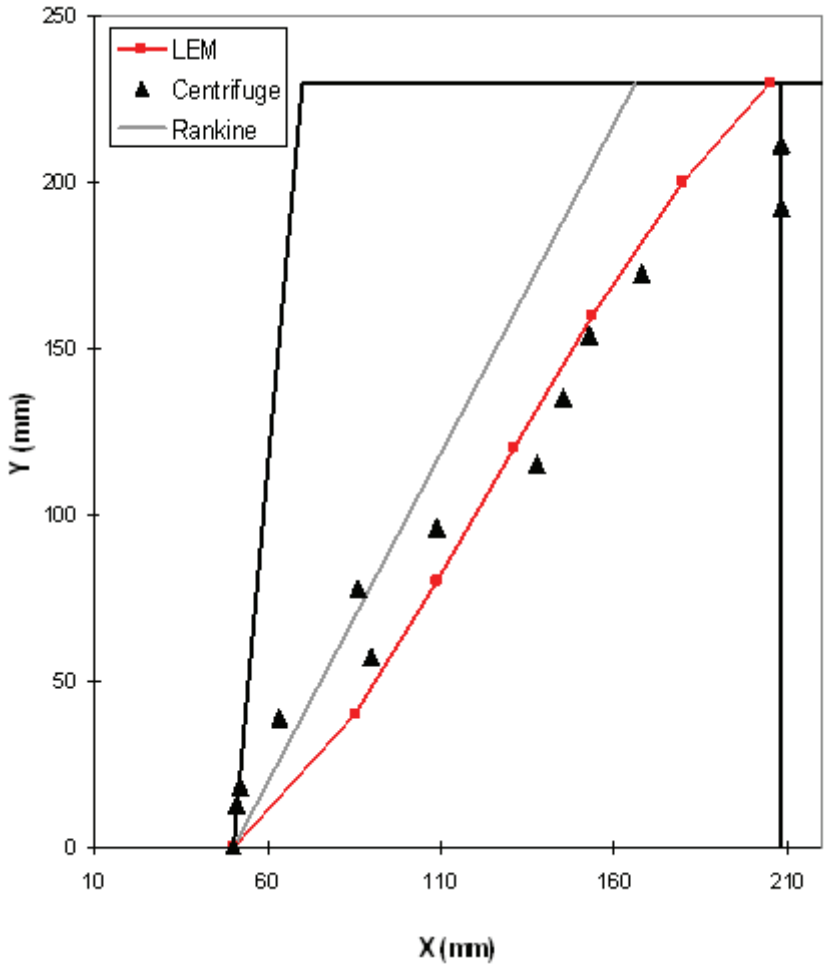

Figure 4.8: Location of failure surface for Test 2a

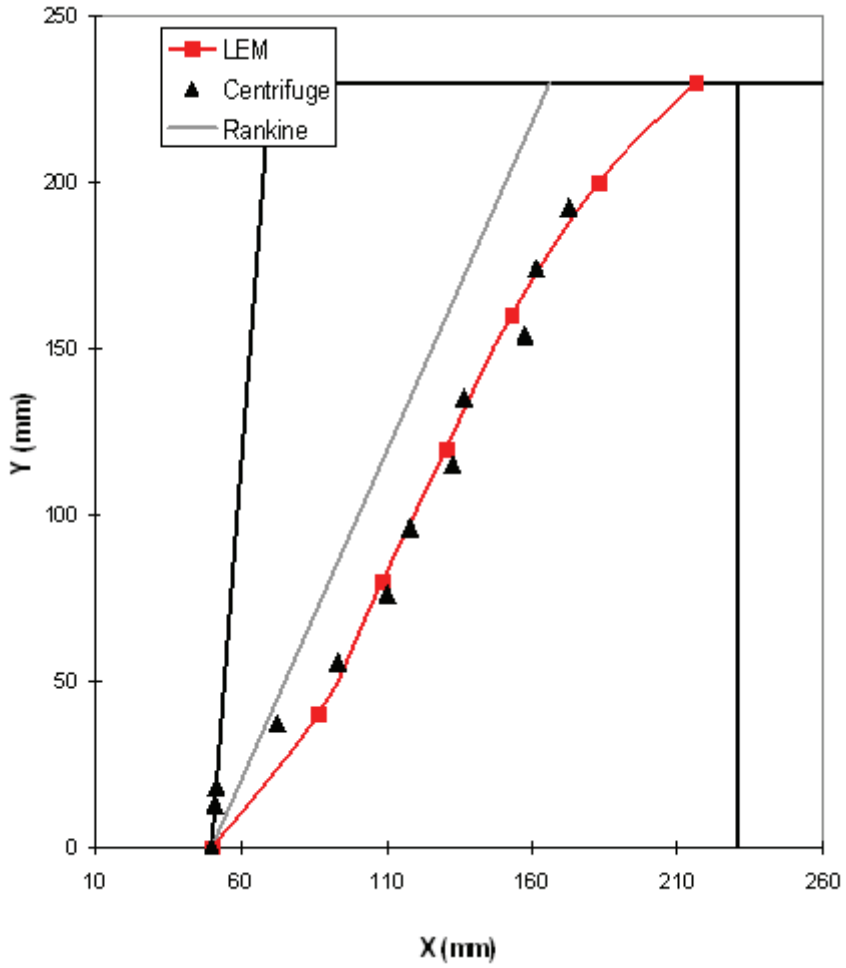

Figure 4.9: Location of failure surface for Test 3b

4.2.3 Normal Stress along Failure Surface

Based on the results from finite element simulation shown in Figure 3.7, there is a zero pressure or no normal stress zone along the interface between the soil and the stable face. This zero pressure zone could cause the backfill material to settle into the crack, as observed from centrifuge test, leading to the instability and failure of the wall. The normal stress acting on the interface between wall and stable face was also examined from the results of limit equilibrium analysis.

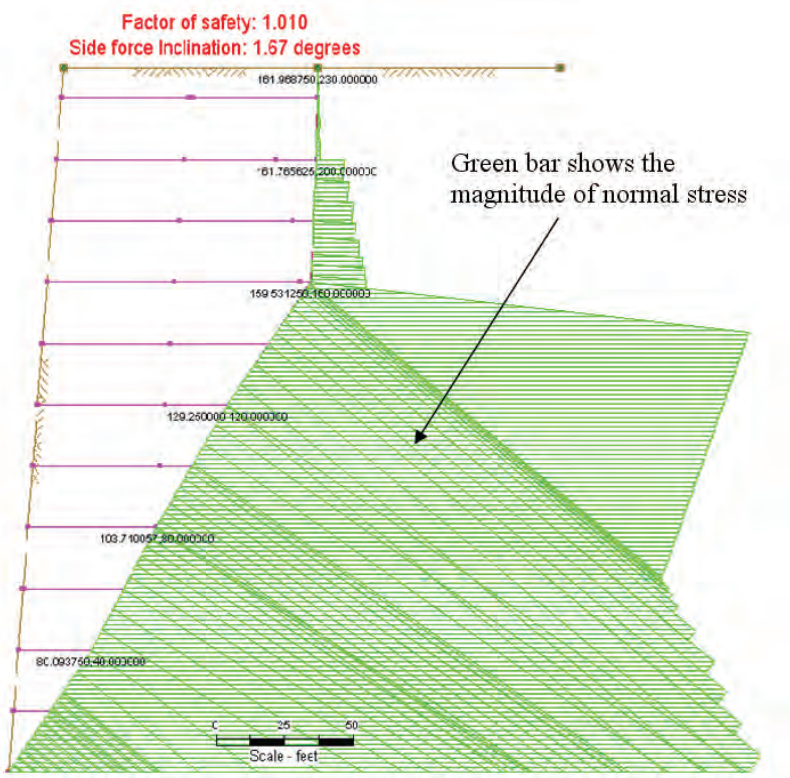

Figure 4.10: Normal stress along the failure surface

Figure 4.10 shows the normal stresses along the failure surface from UTEXAS post-processing output file. The normal stresses are less at the upper part of the failure surface (along interface between the soil and stable face) compared to the normal stresses at the lower part of the failure surface. This observation agrees with the observation from finite element simulation.

4.3 Parametric Studies

Two parametric studies, based on the calibrated limit equilibrium model, are discussed in this section.

4.3.1 Effect of the Reinforcement Pullout Resistance

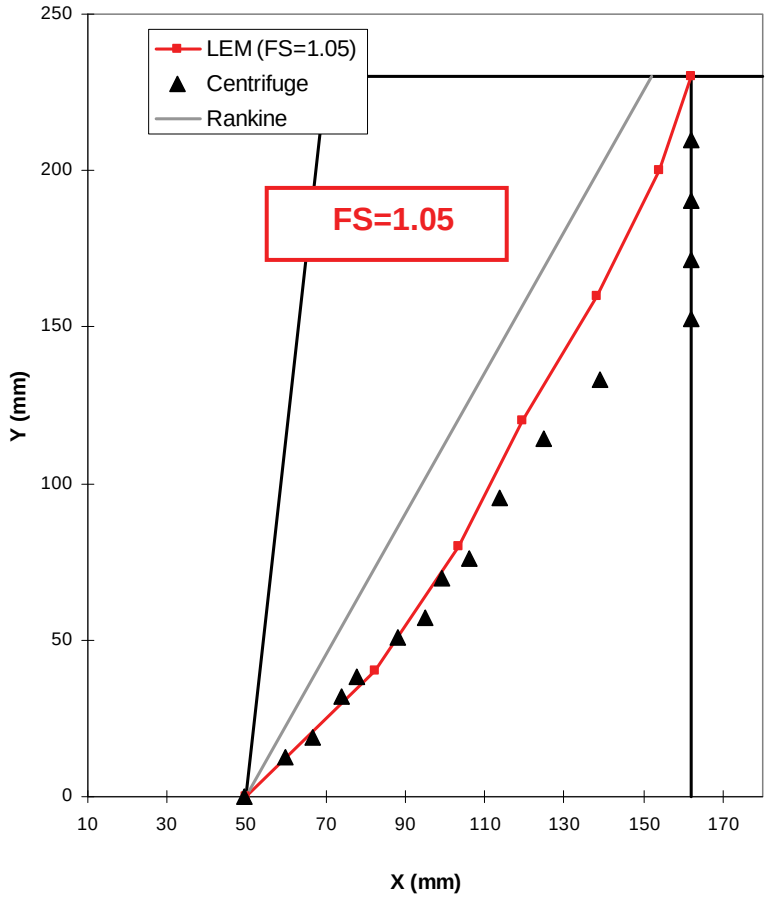

Figure 4.11: The factor of safety and location of failure surface by ignoring the slope part of tensile force in reinforcement

In Figure 4.2, the tensile force of reinforcement was modeled by two portions, a uniform portion with the confined tensile strength and a linearly varying portion by considering the pullout resistance. In this section, a parametric study was performed to evaluate the effect of the approach used to simulate the pullout resistance along the reinforcement. In this parametric study, the tensile forces of reinforcements in each layer were assigned as a constant value (0.225 kN/m) uniformly distributed through the entire reinforcement. In the other words, the varying portion in Figure 4.2 was ignored in this analysis.

The results (factor of safety and location of failure surface) are shown in Figure 4.11. The factor of safety increases slightly from 1.01 to 1.05. This is probably due to the increase of tensile force of reinforcement obtained by ignoring the varying portion. It was further observed that the upper part of failure surface departs from the failure surface measured from centrifuge test toward Rankine failure surface; nevertheless, the lower part of the failure surface was still the same as the failure surface measured from the centrifuge test. The difference occurred only in the upper portion of the failure surface, shown in Figure 4.1. The change of tensile force distribution along the reinforcement obtained by neglecting the varying portion of the tensile

force was small in most of the reinforcement layers but significant in the upper three reinforcement layers.

The critical failure surface has a nature of seeking the location of soil with the low strength or the low tensile force of reinforcement to pass through; however, by unifying tensile force along the reinforcement, it makes the critical failure surface not have to pass through the tail part of the reinforcement, which has a lower tensile force. Consequently, the predicted failure surface in upper layers of reinforcements departs from the measured failure surface. Additionally, the location of the predicted failure surface is unconservative compared to measured failure surface for the purposes of pullout evaluation. Based on this parametric study, use of a rigorous approach to simulate pullout resistance along the reinforcement is proved important to capture the actual location of failure surface.

4.3.2 Effect of Tensile Force Suggested by FHWA Design Guidelines

In this section, a parametric study was performed to examine the use of tensile force, as suggested by FHWA design guidelines (Elias et al, 2001), in the limit equilibrium analyses. FHWA design guidelines recommend using Equation 4.4 to compute the required allowable tensile force for each layer of reinforcement as follows:

$$T_{allowable,i} = FS_{breakage}\left(\frac{k_r}{K_a}\right)K_a \gamma z S_v \qquad \text{Eq. (4.4)}$$

where:

$T_{allowable}$ is the allowable tensile force per unit width of reinforcement at a given layer, i,
$FS_{breakage}$ is the factor of safety against breakage (general assigned as 1.5),
k_r/K_a is the normalized horizontal earth pressure coefficient,
K_a is the theoretical Rankine active earth pressure coefficient,
γ is the unit weight of the reinforced backfill,
z is the depth of the layer of reinforcement below the top of the backfill,
S_v is the vertical spacing between layers of reinforcement,

The normalized horizontal earth pressure coefficient (k_r/K_a) varies with the type of reinforcement, as determined according to Figure 4.12. As shown in Figure 4.12, the k_r/K_a for geosynthetic reinforced wall has a value 1.0 and remains constant throughout the depth of wall. The final computed tensile forces increases linearly from the topmost layer of reinforcement to the bottommost layer of reinforcement. The tensile force calculated at the bottom layer of reinforcement was 0.85 kN/m and used as an input tensile force for limit equilibrium analysis. The effect of simulating pullout resistance was included in this analysis.

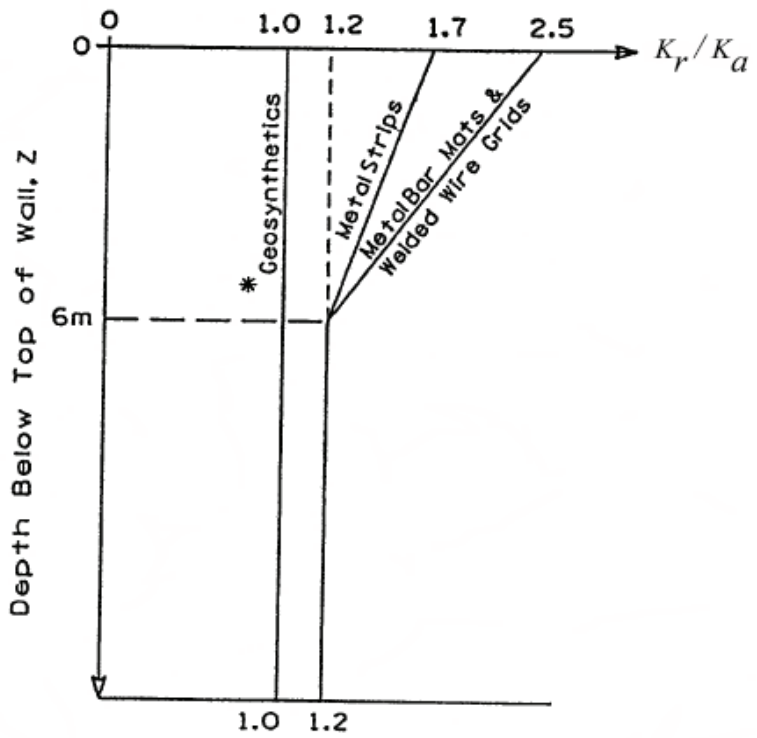

Figure 4.12: Variation of stress ratio with depth in a MSE wall (Elias et al., 2001)

The results of limit equilibrium analysis are shown in Figure 4.13. The factor of safety increases from 1.01 to 2.66 when increasing in the tensile forces from 0.225 kN/m to 0.85 kN/m. The factor of safety was calculated as 2.66, implying that the wall is stable. The failure surface is below the measured failure surface from centrifuge test; however this discrepancy is considered acceptable because the calculated failure surface is on the conservative side for designing the failure surface to compute the resistance against pullout.

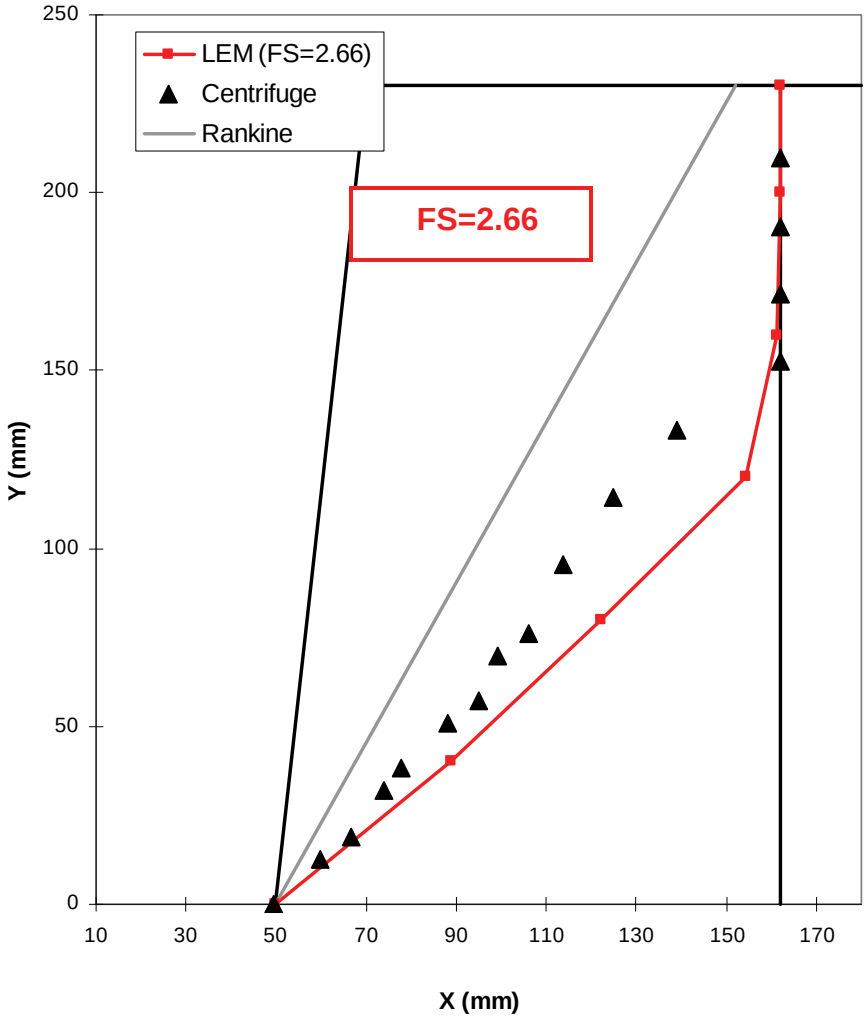

Figure 4.13: The factor of safety and location of failure surface by using the tensile force suggested by the FHWA Design Guidelines

4.4 Effect of Aspect Ratio on the Location of the Failure Surface

The inclination angle of the failure surface is an important outcome of the limit equilibrium analysis and it is also a valuable design parameter to calculate the factor of safety against pullout. For the case of narrow MSE walls, the inclination angle is symbolized as θ_f and illustrated in the Figure 4.14.

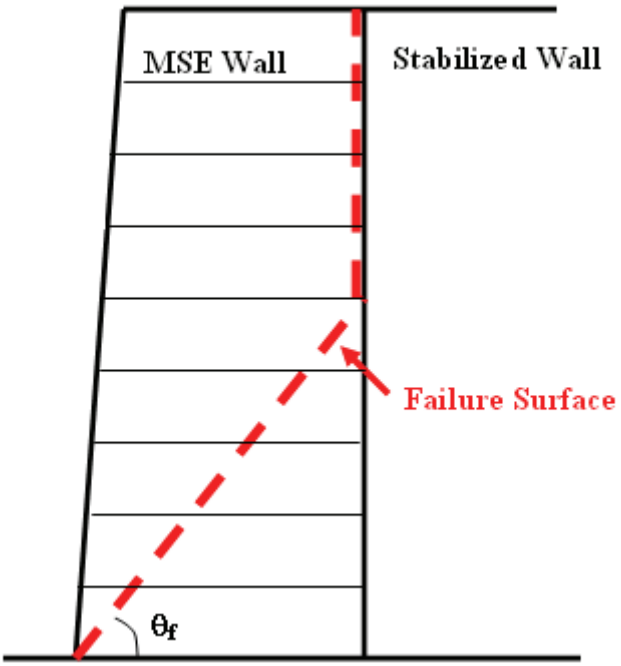

Figure 4.14: Illustration of inclination angle of failure surface

The inclination angles of failure surfaces from Tests 2a, 2b, and 3b were measured based on the approach described above. Both of the results from centrifuge test and limit equilibrium analysis are shown in Figure 4.15. A parametric study of the inclination angle of failure surface at wall aspect ratio 0.3 was conducted. The purpose of this parametric study is to extend the inclination angle to the wall aspect ratio of 0.3 at which the wall failure mode transfers for compound failure to external failure.

Figure 4.15 shows a chart of inclination angles of failure surfaces changing with various aspect ratios. A best-fit-line regression using data from limit equilibrium analyses is presented in Figure 4.15. The regression line decreases as wall aspect ratio decreases. The dashed horizontal line represents the inclination angle of Rankine's failure plane suggested by FHWA design guidelines for shored mechanically stabilized earth (SMSE) wall systems (Morrison, 2006). The inclination angle suggested by FHWA design guidelines based on Rankine's failure plane appears to overestimate the inclination angle of failure surface observed from centrifuge tests and limit equilibrium analyses. Furthermore, the approach suggested by FHWA design guidelines estimates factor of safety against pullout on the unconservative side.

The reason for the difference in the failure surface from theoretical Rankine's failure surface can be attributed to the following factors:

- Arching Effect (Interaction with Stable Face)
- Boundary Constraint (Reduced Aspect Ratio)
- Presence of Reinforcement

These factors constrain the degree of freedom of the soil mass and, thereby, increase the strength of soil. As a result, the soil friction angle increases and inclination angle of failure surface decreases (with respect to the inclination angle of Rankine's failure surface).

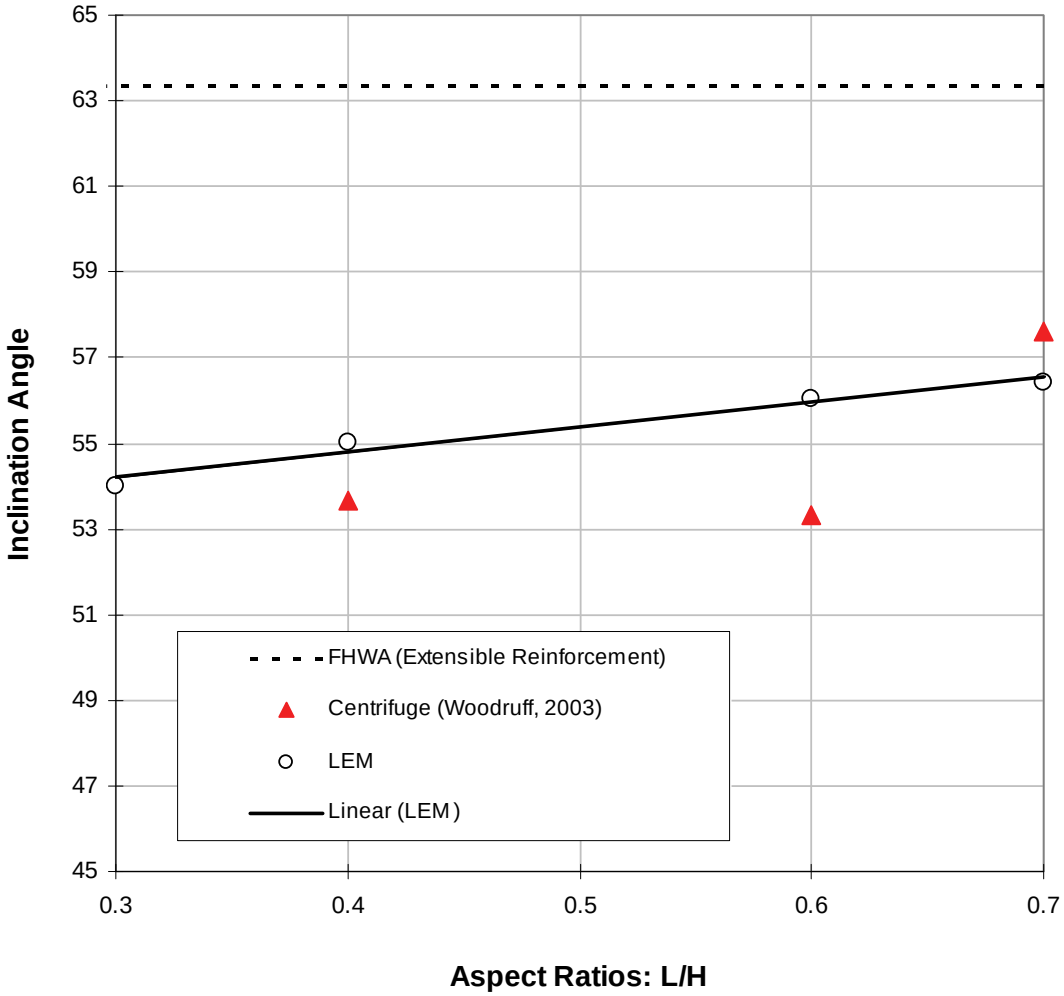

Figure 4.15: Inclination angles of failure surfaces versus various aspect ratios

Figure 4.15 was developed based on only one value of soil friction angle. In order to apply the results of this study to a wide range of soil types, the information in Figure 4.15 was normalized by 45+ϕ'/2, the inclination angle of Rankine's failure plane. In Figure 4.16, the inclination angle starts around 90 percent of the inclination angle of Rankine's failure surface at wall aspect ratio 0.7 and decreases slightly to 85 percent at wall aspect ratio 0.3. An extra data point of centrifuge test reported by FHWA SMSE wall design guidelines was included in the Figure 4.16. This data point seems to follow the trend predicted by Woodruff (2003) centrifuge tests and limit equilibrium analyses.

Woodruff (2003) observed that when the wall aspect ratio decreased below 0.3, the failure mode changed from compound failure to external failure; however, in some cases, even though the wall aspect ratio below 0.2 but the external failure is not going to happen. This may be because the external failure can be prevented by attaching reinforcement to the shored wall or extending upper layers of reinforcements to the top of shored wall. The wall aspect ratio (x-axis) in Figure 4.16 is extended to a value of 0.2. The intension is to include the failure surface of wall aspect ratio from 0.2 to 0.3 for the cases discussed above.

The design chart provides information regarding the failure surface and the embedment length of reinforcement. This can be used to calculate the factor of safety against pullout. For

narrow wall with aspect ratio for 0.6 to 0.3, the wall failure mode is a compound failure. This failure mode often predicts the factor of safety against pullout as less than 1.0 in the top layers. In other words, the wall would fail locally by pullout or pull way of reinforcements. Therefore, remedial measures are required to prevent the local failure; for example, by attaching the reinforcement to the shored wall.

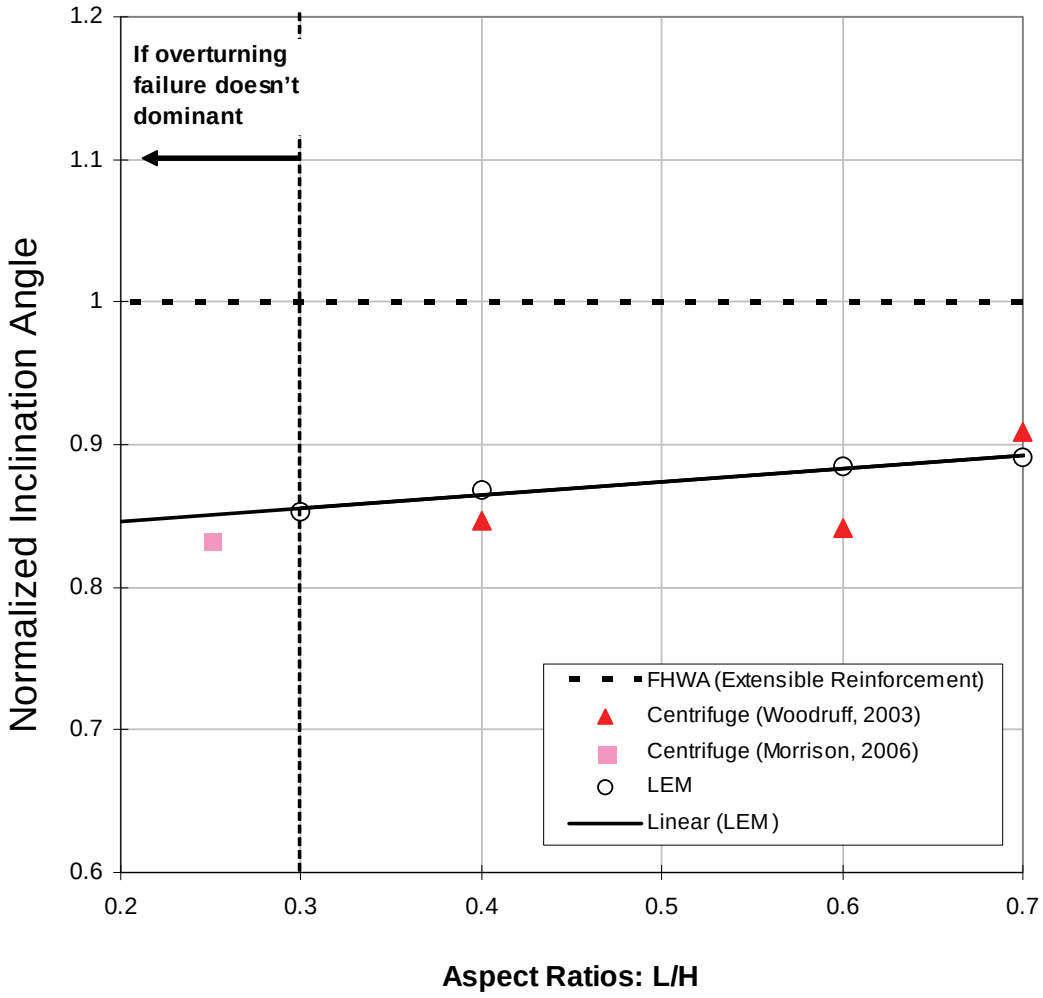

Figure 4.16: Normalized inclination angles

4.5 Conclusions

This chapter presented limit equilibrium analyses to model the centrifuge test of narrow MSE walls. The results predicted by the limit equilibrium model were compared to the results from the centrifuge test. The predicted results were in agreement with the centrifuge experimental results. The calibrated model could now serve as the basis for the design of narrow MSW walls using limit equilibrium. The study also showed that using the inclination angle as obtained using Rankine failure plane for narrow wall systems results in an overestimation of the actual inclination angle.

Parametric studies were conducted to investigate the effect of pullout resistance along the reinforcement as well as the effect of tensile force calculated based on FHWA design guidelines. The parametric study showed the effect of pullout resistance along the reinforcement was important and should be included in the analysis to capture the true location of failure surface. The parametric study on the effect of tensile force suggested by FHWA design guidelines revealed that a wall designed by using the tensile force suggested by FHWA design guidelines was fair stable and the calculated failure surface was in the safe side of design for resistance against pullout.

A design chart for inclination angle of failure surface versus various wall aspect ratios was proposed. This design chart provides the information on the location of the failure surface and the embedment length of reinforcement needed to calculate the factor of safety against pullout. Further design considerations may be needed to improve the stability of the wall, for example, attaching reinforcement to the shored wall or extending upper layers of reinforcements to the top of shored wall. For future study, these design considerations could be evaluated using the limit equilibrium method.

5. Overall Conclusions

This report presents an investigation of the failure mechanisms and characteristics of narrow wall systems; a MSE wall has an aspect ratio (L/H) less than 0.70 and placed in front of a stable wall. Finite element and limit equilibrium analyses were conducted to simulate the centrifuge tests of narrow MSE walls with extensible reinforcements. Both methods were considered useful tools for engineering application. The results of numerical simulations were initially calibrated by the experimental results from centrifuge tests. Subsequently, a series of parametric studies was performed based on the validity of the calibrated numerical models. The behavior and mechanics of the narrow MSE wall were observed and understood through parametric studies.

A summary and the conclusions that can be drawn from this reported are:

Finite Element Analysis

- Finite element analyses were conducted to model centrifuge tests of a narrow MSE wall with extensible reinforcements. The purposes of this study were to validate the proposed finite element model and to study the mechanics of failure initiated by a zero pressure zone. The understanding of the mechanisms and development of a zero pressure zone were confirmed.
- The finite element program Plaxis version 8.2 (Plaxis, 2005) was used. The material properties, modeling methods and procedures were explicitly discussed in Chapter 3.
- The results predicted by the proposed finite element model were compared to the results from centrifuge test under working stress and failure condition. The results from physical and numerical models were in a good agreement. The procedure of finite element modeling narrow MSE walls could serve as basis for subsequent practical applications.
- The stress information from finite element analysis indicated that the “trench” observed from centrifuge test corresponds to a zero pressure zone at the interface between stabilized and MSE wall. This zone extends farther below the crest as the wall width became narrower and approximately reached the bottom of wall at wall aspect ratio 0.25. As a result of this zero pressure zone, the backfill of MSE walls show a tendency to sink into this trench and ultimately cause the failure of the MSE wall.
- Design considerations based on the results from finite element simulation were proposed to improve the stability of the narrow MSE wall. This includes attaching reinforcements to the stable face or extending upper reinforcements over the existing wall to eliminate the developing of a zero pressure zone at interface; using rigid face instead of flexible face to limit the deformation at front face; improving the strength of backfill and foundation.

Limit Equilibrium Analysis

- Limit equilibrium analyses were used to model centrifuge tests of a narrow MSE wall with extensible reinforcements. The purposes of this study were to verify the proposed limit equilibrium model and to investigate the failure surface and the factor of safety for a narrow wall. The study adds basis for designing a narrow MSE wall against pullout failure and for checking the global stability.
- The limit equilibrium analyses were performed by using the program, UTEXAS4. The material properties, modeling methods and procedures were explicitly discussed in Chapter 4.
- The results predicted by the limit equilibrium model were compared to the results from the centrifuge test. The results from physical and numerical models matched well. The procedure of limit equilibrium modeling narrow MSE walls could serve as a basis for subsequent practical applications.
- The parametric study showed that the effect of simulating pullout resistance along the reinforcement is important and should be included in the analysis to capture the true location of failure surface.
- The parametric study on the effect of using input tensile forces, as suggested by FHWA design guidelines revealed that a wall designed using the tensile force suggested by FHWA design guidelines was stable and the calculated failure surface was in the safe side of design for pullout resistance.
- A design chart of inclination angle of failure surface versus various wall aspect ratios was developed. The inclination angle ranges from approximately 90 percent of the inclination angle of Rankine's failure surface for wall aspect ratio of 0.7 and decreases slightly to 85 percent for wall aspect ratio of 0.3. This chart is useful for engineers to design the failure surface in a narrow MSE wall and, therefore, to calculate the factor of safety against pullout.

References

Arriaga, Fabiana (2003), “Response of geosynthetic-reinforced structures under working stress and failure conditions.” Thesis submitted in partial fulfillment of the requirements for the degree of Doctor of Philosophy, Department of Civil Engineering, University of Colorado, Boulder, Colorado.

Bolton, M.D., (1986), “The strength and dilatancy of sands,” *Geotechnique*, Vol. 36, No. 1, pp. 65-78.

Elias, V., Christopher, B.R., and Berg, R.R., (2001), "Mechanically Stabilized Earth Walls and Reinforced Soil Slopes Design and Construction Guidelines," *Report No. FHWA-NHI-00-043*, National Highway Institute, Federal Highway Administration, Washington, D.C. March.

Frydman, S. and Keissar, I., (1987), "Earth pressure on retaining walls near rock faces," *Journal of Geotechnical Engineering*, ASCE, Vol. 113, No. 6, June, pp. 586-599.

Kniss, K., Wright, S., Zornberg, J.G., and Yang, K.-H., “Design Considerations for MSE Retaining Walls Constructed in Confined Spaces” *Center for Transportation Research (CTR), Report no. 0-5506-1*, Austin, Texas, October 2007.

Ko, H.Y. (1998), “Summary of the state-of-the-art in centrifuge model testing,” Proc. Intl. Conf. Centrifuges in Soil Mechanics, James and Schofield (eds), p. 11-18.

Lawson, C.R., and Yee, T.W., (2005), "Reinforced soil retaining walls with constrained reinforced fill zones," *Proceedings, Geo-Frontiers 2005*, ASCE Geo-Institute Conference, pp. 2721-2734.

Leshchinsky, D., Hu, Y. and Han, J., (2004), " Limited reinforced space in segmental retaining walls," *Geotextiles and Geomembranes*, Vol. 22, No. 6, pp. 543-553.

Li, C., (2002), “Experimental studies on fiber-reinforced soil”, *University of Colorado Research Report*.

Marachi, N., Duncan, J.M., Chan, C., and Seed, H.B., (1981). “Plane-strain testing of sand”, Laboratory Shear Strength of Soil, Yong, R.N. and Townsend, F.C., Editors, ASTM Special Technical Publication 740, proceedings of a symposium held in Chicago, Illinois, USA, June 1980, pp. 294-302

Morrison, K.F., Harrison, F.E., Collin, J.G., Dodds, A., Arndt, B. (2006), “Shored Mechanically Stabilized Earth (SMSE) Wall Systems Design Guidelines,” *Report No.FHWA-CFL/TD-06-001*, Federal Highway Administration, Central Federal Lands Highway Division.

PLAXIS (2005). *Plaxis Finite Element Code for Soil and Rock Analyses*, Version 8.2, P.O. Box 572, 2600 AN Delft, The Netherlands (Distributed in the United States by GeoComp Corporation, Boxborough, MA).

Spencer, E (1967). "A method of analysis of the stability of embankments assuming parallel inter-slice forces." Geotechnique, 24(4), p. 661-665.

Take, W.A. and Valsangkar (2001), "Earth pressures on unyielding retaining walls of narrow backfill width," *Can. Geotech. Journal*, Vol.38, pp.1220-1230.

Woodruff, R. (2003), "Centrifuge modeling of MSE-shoring composite walls," Master Thesis, Department of Civil Engineering, the University of Colorado, Boulder.

Wright, S.G. (1999), "UTEXAS4 A Computer Program for Slope Stability Calculations." Shinoak Software, Austin, Texas, September, 221p.

Zornberg, J.G., Mitchell, J.K., and Sitar, N. (1997), "Testing of reinforced slopes in a geotechnical centrifuge," Geotech. Testing Journal., Vol.20, No. 4, pp. 470-480.

Appendix A. Modeling a Flexible Wall Face

A.1 Introduction

This appendix reports a method of modeling the flexible wall face, i.e., the wall face made up of geosynthetics wrap around. Although several possible methods have been suggested for the modeling a flexible wall face in the literature, because of the obstacle of suggested methods and the limited capacity of Plaxis, using a plate element to model the flexible wall face was adopted.

A plate element has two input parameters; the axial stiffness, EA, and the bending stiffness, EI. The plate element is competent to model a wide variety of facing materials from very flexible like a geosynthetic fabric to very rigid like a concrete block. For the rigid face, the original material properties provided directly form laboratory or factory are used as input values for the plate element. Unfortunately, it is not the case for the flexible face. Only the value of EA is provided for the geosynthetics material and the value of EI is usually negligible. Therefore, a parametric study is needed to find out appropriate input stiffnesses for the plate element to represent the flexible wall face.

The arrangement of this appendix starts by reviewing all possible methods of simulating the flexible facing elements. Then, the modeling of the flexible wall face using the plate element is presented. A technique of normalization, based on engineering beam theory, is introduced to normalize the bending stiffness and normal stiffness of the plate element. The purpose of normalization is expected to expand the application of this study to a wide range of wall geometry and backfill material. A parametric study to find appropriate normalized stiffnesses to represent the flexible wall face is discussed in the last part of appendix.

A.2 Possible Methods

Four possible ways were considered to model the flexible wall face: 1) adding additional elements with enough cohesive strength to withstand the earth pressure created by the granular backfill, 2) applying an external pressure perpendicular to the face, 3) using a membrane element to model the facing material, and 4) introducing a plate element to simulate the facing material. Because of some limitations that occurred when considering the first three items, item 4 using a plate element was finally selected for modeling the flexible wall face. The obstacles of first three items are as follows:

1. Using cohesive material to support the granular material has no realistic application and would require determining the appropriate cohesive strength required to support the backfill for a given simulation and the effect of the cohesive material on the lateral earth pressure and consequently the reinforcement.
2. Applying an external pressure perpendicular to the face has the same concern as applying cohesive material. Furthermore, the lateral earth pressure in the soil will react to the pressure at the face rather than find its own equilibrium. Therefore, the results are controlled by the applied pressure and not by the behavior of the soil mass.
3. A member element is the element that only has axial stiffness but is designed to bear lateral force as well as axial force. The lateral force can be equilibrated by the deflection and the

developed axial force of the element. A member element might be an approach that could be considered; however, Plaxis does not have such an element and, thus, this approach could not be used.

A.3 Plate Elements

In Plaxis, Plates are structural elements used to model slender structures with bending stiffness and normal stiffness. The plate element in Plaxis is also referred to as beam element in other finite element programs. It has both length and width and can react to both tensile and compressive stresses. The behavior of a plate is defined by the axial stiffness, EA, and bending stiffness, EI. For both axisymmetric and plane stain models, the values of EA and EI relate to a stiffness per unit width in the out-of-plane direction. The axial stiffness, EA, is given in force per unit width [F/L] and the bending stiffness, EI, is given in force length squared per unit width [FL^2/L]. Examples of five-node and three-node plate elements are shown in Figure A1 below. Plate elements are given an equivalent thickness based on the input values of EA and EI. Equation B1 lists the equation to calculate equivalent thickness of plate elements for rectangular cross section.

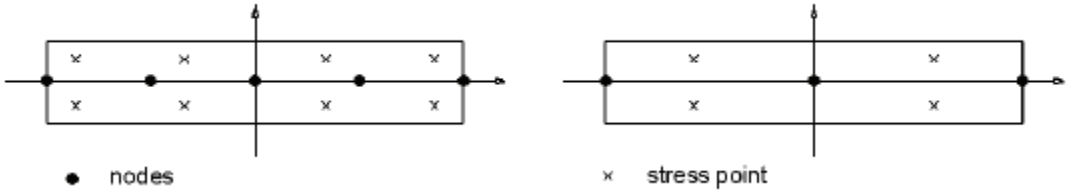

(a) (b)

FigureA.1 ibution of nodes and stress points in plate ele 5-node (b) 3-node

$$deq = \sqrt{12\frac{EI}{EA}} \qquad \text{Eq. (A1)}$$

A.4 Normalization of EA and EI

Finding appropriate values of EA and EI is the main purpose of this study; however, the EA and EI for flexible wall face could be varied with various wall geometry; for example the EA and EI would be different between 1 meter and 0.5 meter vertical spacing of wall. The EA and EI are required to be normalized with the result that the normalized values can be applicable for any wall geometries. The plate is a structural element, thus defined properties and mechanical behavior follow well with engineering beam theory. Herein, engineering beam theory is used as the basis of normalization.

A.4.1 Normalization of EA

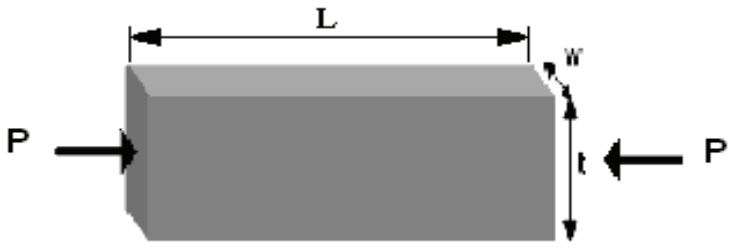

Figure A.2: Axial loading of a beam

Figure A2 illustrates a beam element bearing an axial loading. Based on engineering beam theory, the change in length due to an axial force on the beam is given by Equation A2.

$$\Delta = \frac{PL}{EA} \qquad \text{Eq. (A2)}$$

where:

Δ is the change in length of the beam;
P is the axial force applied to the beam;
L is the length of the beam;
E is the modulus of elasticity or Young's modulus;
A is the cross-sectional area of the beam.

The axial force load on the plate in the simulations can be treated as force due to backfill overburden pressure. The overburden pressure would be the greatest at bottom of the wall; therefore, the load P can be substituted by γHA. A is the cross-sectional area of the beam and has two dimensions; t and w (see Figure A2.). Because we are dealing with unit length out of plane, the length of plate width, w, is a unit and included implicit in the equation. If the change in length is normalized by the original length of the beam, the result is a non-dimensional value that is a function of the axial stiffness, EA of the plate, shown in Equation A3. The following equation can also be view as the developed strain caused by the applied stress.

$$\frac{\Delta}{L} = \frac{\gamma Ht}{EA} \qquad \text{Eq. (A3)}$$

where:

t is the thickness of the beam

Based on the inverse of Equation A3, the normalized axial stiffness, N_{EA}, is proposed in Equation A4. The physical meaning of N_{EA} is the inverse of developed strain caused by the applied stress.

$$N_{EA} = \frac{EA}{\gamma Ht} \qquad \text{Eq. (A4)}$$

A.4.2 Normalization of EI

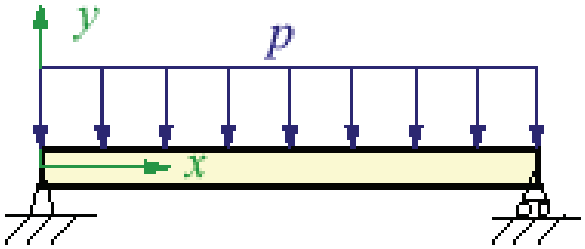

Figure A.3: Example of simply supported beam with distributed load P

Figure A3 shows a beam element bearing a distributed lateral loading. If the plate element is treated as a continuous simply supported beam, based on engineering beam theory, the lateral deflection of the beam resulting from a distributed load acting normal to the beam is given by Equation A5.

$$\delta = \frac{5PL^4}{384EI} \qquad \text{Eq. (A5)}$$

where:

δ is the deflection at the center of the beam
P is the applied distributed load per unit length,
L is the length of the beam,
E is the modulus of elasticity or Young's modulus, and
I is the moment of inertia of the beam.

The applied distributed load on the plate in the simulations can be conceived as lateral earth pressure. At the bottom of the wall, the applied force would be the greatest so the lateral earth pressure at bottom is considered; therefore, the distributed load P can be substituted by $k\gamma Hw$, where k is the lateral earth pressure coefficient at bottom of the wall. Again w is a unit and included implicit in the equation. If the deflection is normalized by the length of the beam, the result is a non-dimensional value that is a function of the bending stiffness, EI, of the plate, shown in Equation A6.

$$\frac{\delta}{L} = \frac{5k\gamma HL^4}{384EI} \qquad \text{Eq. (A6)}$$

Based on the inverse of Equation A6 and neglect of non-dimensional quantity, $\frac{5k}{384}$, the normalized bending stiffness, N_{EI}, is proposed in Equation A7.

$$N_{EI} = \frac{EI}{\gamma HL^4} \qquad \text{Eq. (A7)}$$

This normalized axial and bending stiffness, N_{EA} and N_{EI}, will be used for following parameter studies to find out the appropriate values to represent the flexible wall face.

A.5 Parametric Study

In this section, a series of parametric study of N_{EA} and N_{EI} was performed to find the appropriate values to simulate the flexible wall face. The finite element model, showed in Figure A4, is a 10-m high wall and has ten layers of reinforcement. The backfill was modeled by Mohr-Coulomb model with the input values of frictional angle 36 degree and unit weight 16 kN/m^3. Reinforcement was simulated by linear elastic model with elastic axial stiffness 2000 kN/m. Total fixity was imposed to simulate the stable face and rigid foundation. Interface element was placed between backfill/wall face and backfill/stable face to capture the soil structure interaction. The material properties of an interface element corresponded with backfill properties. The strength of the interface was reduced by one-third of the strength of backfill material.

A plate element was used to model the facing element. Each facing element was 1 m height. Only the axial and bending stiffnesses in plate element were changed during parameter studies to investigate the influence of axial and bending stiffnesses on earth pressure adjacent to the wall face. The target was set to reduce the values of axial and bending stiffnesses in the plate element until found the minimum values of earth pressure adjacent to the wall face. In the condition of minimum earth pressure, we can say that the values of axial and bending stiffnesses are appropriate for modeling the flexible wall face. The procedure of parametric study involves the following:

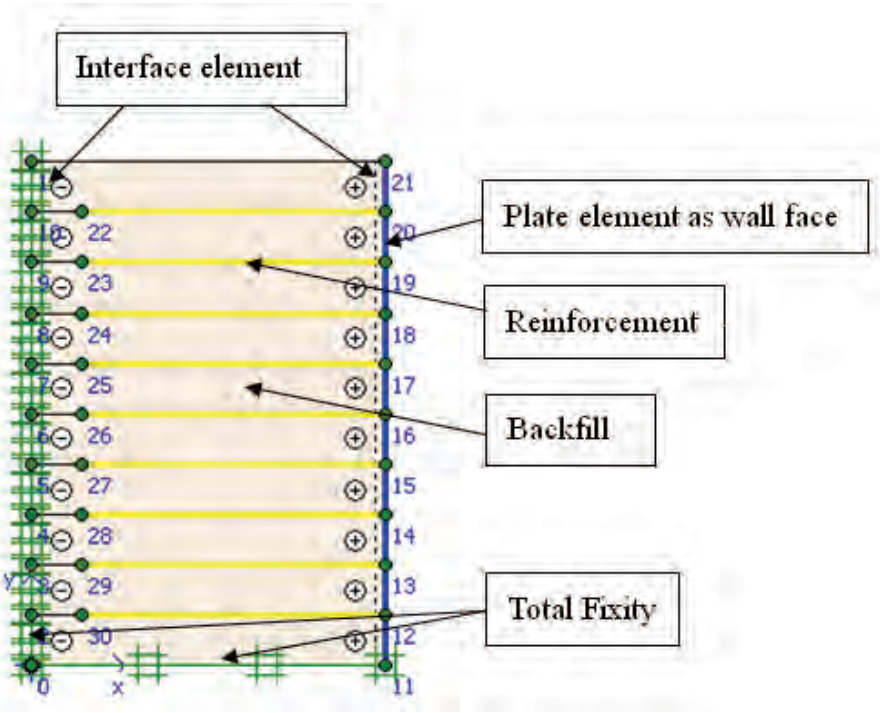

Figure A.4: Finite element model for flexible wall face

Step 1. Three series of simulations were performed corresponding to three values of EA, 10000, 3000 and 500 kN/m. The selection of these values was trying to cover a wide range of EA as possible. In each series of simulation, the values of EA were fixed and the values of EI were changed. The final product for each simulation was the equivalent earth pressure coefficient adjacent to the wall face. The equivalent earth pressure coefficient adjacent to the wall face was calculated by integrating the earth pressure adjacent to the wall face along the entire vertical profile and dividing $1/2\gamma H^2$. Figure A5 plots the equivalent earth pressure coefficient adjacent to the wall face normalized by Rankine active earth pressure coefficient versus the various values of normalized bending stiffness, N_{EI}. The values of N_{EI} were calculated by Equation A7 based on input EI values, wall geometries and backfill properties.

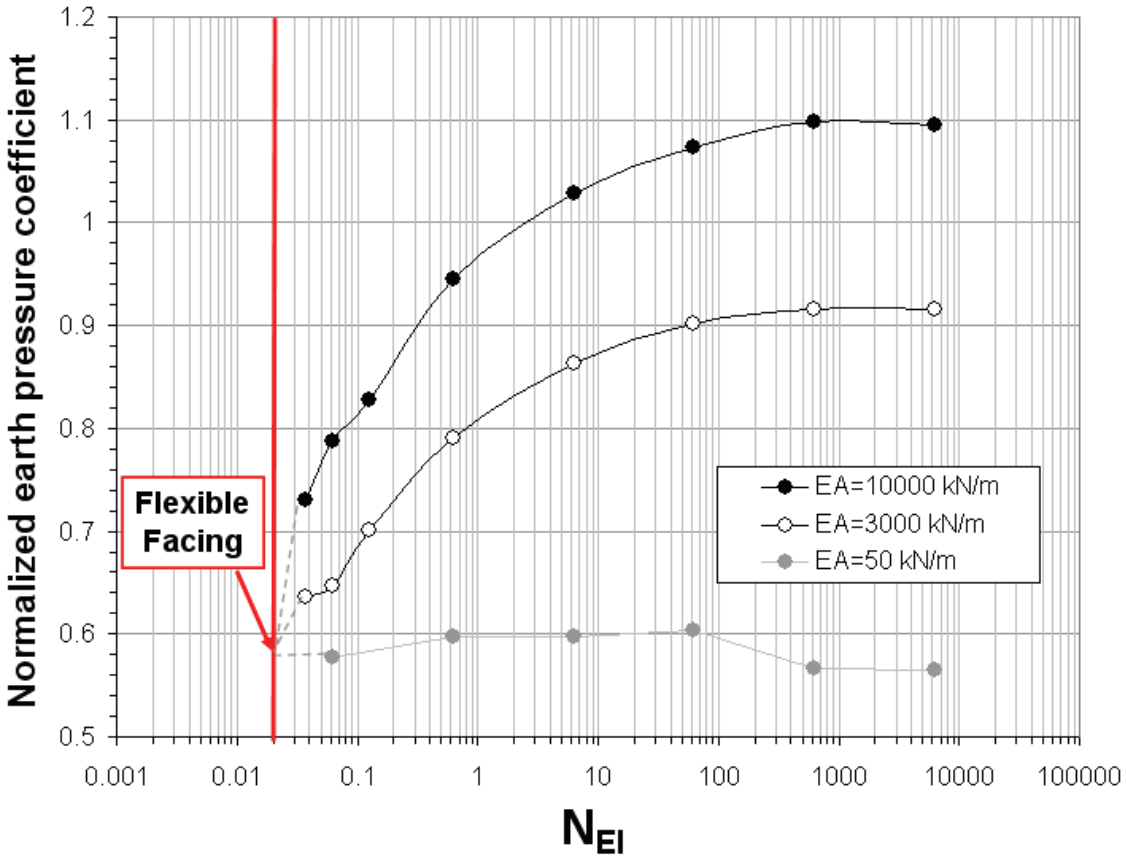

Figure A.5: Graph used to determine the values of N_{EI} for a plate

Several observations were made from Figure A5. First, the normalized earth pressure coefficient decreased with the decrease of N_{EI}. This trend was clear for EA equal to 10000 and 3000 kN/m. For the case of EA equal to 50 kN/m, the trend was not obvious. The possible reason may be, in this case, the axial stiffness of wall face was low enough so the further decreased bending stiffness won't influence the normalized earth pressure coefficient too much. Second, the decrease of the normalized earth pressure coefficient with the decrease of N_{EI} seemed likely to converge at N_{EI} around 0.02 for any values of

EA; consequently, for modeling the flexible face, 0.02 was decided for the value of normalized bending stiffness, N_{EI}.

Step 2. After deciding the values of N_{EI} for flexible face, the next simulation was performed by fixing the N_{EI} at 0.02 and changed the values of EA until find the minimum values of earth pressure adjacent to the wall face. Figure A6 plots the equivalent earth pressure coefficient adjacent to the wall face normalized by Rankine active earth pressure coefficient versus the various values of normalized axial stiffness, N_{EA}. The values of N_{EA} were calculated by Equation A4 based on input EA values, wall geometry and backfill properties. In Equation A4, the thickness, t, of the plate element was calculated by Equation A1 and a unit is assigned for the width, w, of the plate element.

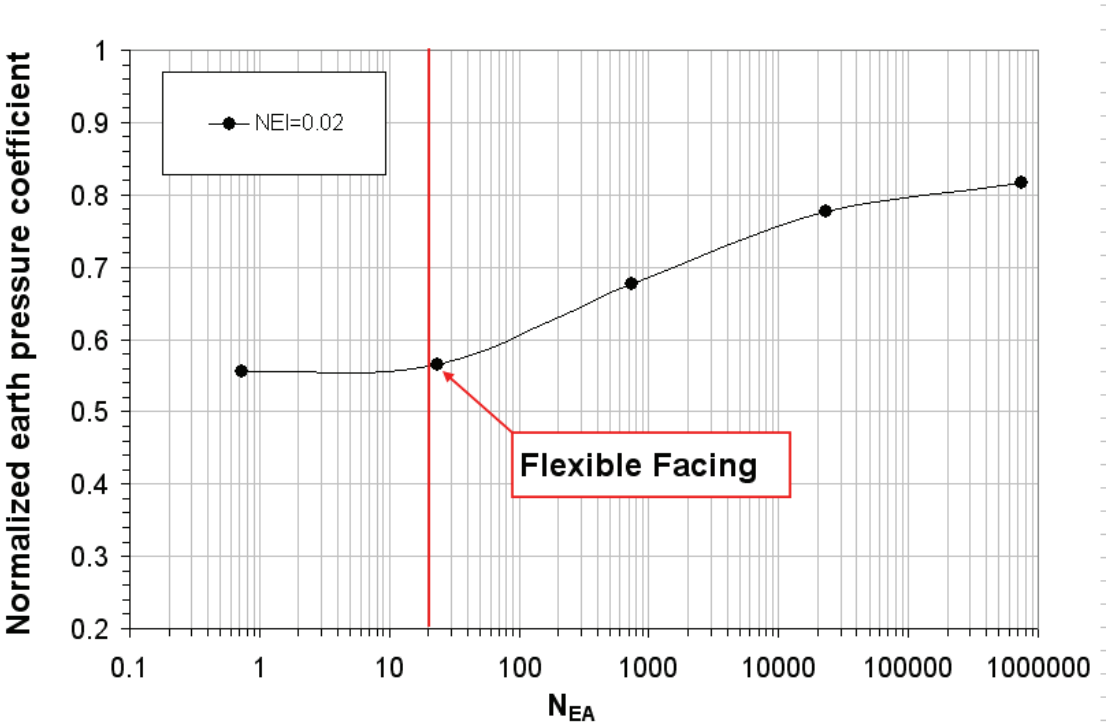

Figure A.6: Graph used to determine the values of NEA for a plate

The decrease of normalized earth pressure coefficient was also observed with the decrease of N_{EA}. The decreasing trend reached asymptote at N_{EA} around 20. When the value of N_{EA} below 20; the normalized earth pressure coefficient was no longer affected by the decrease of axial stiffness; consequently, for modeling the flexible face, 20 was decided for the value of normalized axial stiffness, N_{EA}.

A.6 Summary

In this appendix, a parametric study was performed to model a flexible wall face, like geosynthetics wrap around face. Several possible methods of modeling a flexible wall face were listed and discussed. Because of the obstacle of the suggested methods and limited capacity of Plaxis, using plate element to model the flexible wall face was finally decided. The input parameters, bending stiffness, and normal stiffness of plate element were normalized. The purpose of normalization was intended to apply the normalized values for a wide range of wall

geometries and backfill properties. A series of parametric studies on these two normalized parameters was performed to find appropriate stiffnesses to represent the flexible wall face. The final values of normalized axial stiffness, N_{EA}, and normalized bending stiffness, N_{EI}, are summarized in the Table A1.

Table A.1: Summary of values for normalized axial and bending stiffnesses

	N_{EI}	N_{EA}
Flexible Face	0.02	20

A.7 Example of Calculation

This section shows an example of computing the values of EA and EI to model the flexible wall face of centrifuge test 2b. The centrifuge test has wall height, H, 230 mm, the vertical space of wall face, L, 20 mm, and the unit weight of backfill, γ, 16.05 kN/m^3. Additional, the centrifuge model was spun up to 40g. This effect can be simulated by enlarging wall dimensions 40 times.

The procedure of finding the values of EA and EI are listed as follows:

Step 1. Calculate EI from Equation A.7

Rearrange Equation A.7.

➔ $EI = \gamma H L^4 * N_{EI} = 16.05 * (\frac{230*40}{1000}) * (\frac{20*40}{1000})^4 * 0.02$

➔ EI=1.2 (kNm^2/m)

Step 2. Calculate EA from Equation A.1 and Equation A.4

Substitute Equation A.1 into Equation A.4

➔ $N_{EA} = \frac{EA}{\gamma H \sqrt{12 \frac{EI}{EA}}}$

Rearrange the equation above

➔ $EA = (\gamma H \sqrt{12EI} * N_{EA})^{\frac{2}{3}} = (16.05 * (\frac{230*40}{1000}) * \sqrt{12*1.2} * 20)^{\frac{2}{3}}$

➔ EA=502 (kN/m)